

1 **Modulating p-hydroxycinnamate behavior as a ditopic linker or photoacid in copper(II)**  
2 **complexes with an auxiliary pyridine ligand†**

3  
4  
5  
6 Joan Soldevila-Sanmartín,<sup>a</sup> Teresa Calvet,<sup>b</sup> Merce Font-Bardia,<sup>c</sup> Concepción Domingo,<sup>d</sup> José A.  
7 Ayllón<sup>\*a</sup> and Josefina Pons<sup>\*a</sup>  
8  
9  
10  
11  
12  
13  
14  
15  
16  
17  
18  
19  
20  
21  
22  
23

24 a Departament de Química, Universitat Autònoma de Barcelona, 08193-Bellaterra, Barcelona, Spain. E-  
25 **mail: JoseAntonio.Ayllon@uab.es, Josefina.Pons@uab.es**

26 b Mineralogia, Petrologia i Geologia Aplicada, Universitat de Barcelona, Martí i Franquès s/n, 08028-  
27 Barcelona, Spain

28 c Unitat de Difracció de Raig-X, Centres Científics i Tecnològics de la Universitat de Barcelona  
29 (CCiTUB), Universitat de Barcelona, Solé i Sabarís, 1-3, 08028-Barcelona, Spain

30 d Instituto de Ciencia de los Materiales de Barcelona (CSIC), Campus UAB, 08193 Bellaterra, Spain  
31  
32  
33  
34  
35  
36  
37  
38  
39  
40  
41  
42

43 **ABSTRACT:**

44

45 The reaction of copper(II) acetate monohydrate with p-hydroxycinnamic acid (HpOHcinn) and different  
46 pyridine derivatives (4-tert-butylpyridine, 4-tBupy; 4-acetylpyridine, 4-Acpy; 3-phenylpyridine, 3-Phpy;  
47 4-phenylpyridine, 4-Phpy) was essayed in methanol solvent at room temperature. The crystal structures  
48 of the resulting compounds were elucidated. Their analysis shows that the choice of pyridine ligands  
49 determines different coordination modes of the pOHcinn ligand and the Cu(II) coordination, nuclearity  
50 and geometry. The pOHcinn acts as a monodentate carboxylate ligand in combination with 4-tBupy or  
51 4-Phpy, yielding monomers and dimers, associated by hydrogen bonds into supramolecular networks in  
52 which the phenol group plays a key role. Conversely, in combination with 4-Acpy or 3-Phpy, the phenol  
53 group coordinates directly to the Cu(II), acting as a ditopic ligand and yielding 2D coordination  
54 polymers.

55 The compound containing 3-Phpy shows interesting MeOH–H<sub>2</sub>O reversible exchange behavior. Not  
56 only has the pyridine auxiliary ligand had a tremendous effect on the coordination mode of pOHcinn,  
57 but also its reactivity is influenced. Particularly, in the case of the compound containing 4-Phpy, it  
58 undergoes a photoinduced process, in which the phenol group deprotonates and coordinates to Cu(II) as  
59 a phenoxy ligand. This yields a coordination polymer in which two different dimers alternate, bridged  
60 by the resulting pOcinn ligand. The magneto-structural correlation of this compound is also discussed.

61

62

63

64

65

66

67

68

69

## 70 INTRODUCTION

71

72 The need to cope with the world's energetic demands while preserving our environment has spurred the  
73 search for new functional materials. In this regard, it is remarkable the great amount of interest shown in  
74 porous materials over the last decade. Thus, Metal–Organic Frameworks (MOFs) and Covalent Organic  
75 Frameworks (COFs) have been investigated extensively due to the possibility of tailoring their structure  
76 to meet specific demands,<sup>1,2</sup> some of them being on the doorstep of industrial application.<sup>3</sup> Recently, a  
77 new class of porous materials, based in supramolecular lattices stabilized only by weak intermolecular  
78 forces, specially hydrogen bonds, has been gaining attention.<sup>4–7</sup> They could present several interesting  
79 properties that outperform those of MOFs, such as wet-processing, low energy regeneration and mild  
80 reaction conditions. Despite being held via weak supramolecular forces, correct selection of the number  
81 and position of the intermolecular interactions can yield highly stable materials.<sup>8–10</sup> These materials  
82 could be built from pure organic subunits, and also from discrete coordination complexes. In this  
83 context, *p*-hydroxybenzoic acid (HpOHBz) is an interesting ligand, which includes a phenol functional  
84 group occupying an opposite position with respect to the carboxylic group. In complexes containing this  
85 ligand, the phenol group usually participates in the generation of supramolecular networks via H-  
86 bonds.<sup>11,12</sup> However, it is less common that this –OH group coordinates with metal sites forming 2D  
87 coordination polymers.<sup>13</sup>

88 Recently, our group has shown that, in the [Cu(*p*OHBz)<sub>2</sub>(dPy)<sub>2</sub>] (dPy = 4-Phpy, 4-Bzpy, 3-PhPy)  
89 family of compounds, small changes in the nature and position of the pyridine substituent govern the  
90 different roles of the phenol group of the *p*OHBz ligand: it can be involved in hydrogenbond  
91 interactions that lead to the formation of supramolecular networks, or it can be bonded to the copper  
92 cation, yielding 2D coordination polymers. These previous results clearly suggest the potential of  
93 organic–inorganic building blocks with peripheral phenol groups for the preparation of both  
94 supramolecular and covalent networks.<sup>14</sup> Some of these compounds show incipient porosity. Hence, in  
95 light of the obtained results it was suggested that using ligands with longer distances between the  
96 carboxylate and the phenol functionalities could result in an increase in the overall empty space, an  
97 already successful strategy.<sup>15</sup> The interest into phenol containing ligands is also being fueled by the  
98 widespread occurrence of tyrosyl radicals in metalloproteins with diverse catalytic activity and the  
99 achievement of similar model compounds that show catalytic activity.<sup>16</sup>

100 In this work, we selected (*E*)-3-(4-hydroxyphenyl)-2-propenoic acid (*para*-hydroxycinnamic acid,  
101 HpOHcinn) for the formation of compounds with channels or other cavities, considering that it is quasi-  
102 planar and has a rigid structure. HpOHcinn coordination compounds using Co(II),<sup>17</sup> Cd(II),<sup>18</sup>  
103 Mn(II),<sup>19</sup> Pb(II),<sup>20</sup> Zn(II),<sup>15,21–24</sup> and lanthanides<sup>25–27</sup> as metal centers have been previously  
104 described. Focusing on Cu(II) coordination compounds, to our knowledge five crystal structures have  
105 been described in the literature.<sup>18,28–31</sup> Furthermore, all these examples show the great variability of  
106 coordination modes allowed by this ligand, such as monodentate, bidentate chelate or bidentate bridge

107 and several have channels occupied by solvent molecules. As a result, monomers, dimers, tetramers and  
108 coordination polymers can be synthesized. However, in none of the reported structures the –OH moiety  
109 coordinates to a metal center. Moreover, this work continues studying the effects of the different  
110 auxiliary pyridine ligands in the coordination of the phenol and carboxylate groups. For this purpose, in  
111 combination with HpOHcinn, four pyridines with different sizes and functional groups were chosen: 4-  
112 terbutylpyridine (4-tBupy), 4-acetylpyridine (4-Acpy), 3-phenylpyridine (3-Phpy) and 4-phenylpyridine  
113 (4-Phpy).

114

115

116

## 117 EXPERIMENTAL SECTION

118

### 119 Materials and methods

120 General details. Copper(II) acetate monohydrate ( $\text{Cu}(\text{Ac})_2 \cdot \text{H}_2\text{O}$ ), (E)-3-(4-hydroxyphenyl)-2-propenoic  
121 acid (p-hydroxycinnamic acid, HpOHcinn), 4-tert-butylpyridine (4-tBupy), 4-acetylpyridine (4-Acpy),  
122 3-phenylpyridine (3-Phpy), 4-phenylpyridine (4-Phpy) reagents and methanol (MeOH) were purchased  
123 from Sigma-Aldrich and used without further purification. All the reactions and the manipulation were  
124 carried out in air.

125 Elemental analyses (EA) of C, H and N were carried out on a Euro Vector 3100 instrument. Fourier  
126 transformed infrared (FTIR) spectra were recorded on a Tensor 27 (Bruker) spectrometer, equipped with  
127 an attenuated total reflectance (ATR) accessory model MKII Golden Gate with a diamond window in  
128 the range  $4000\text{--}600\text{ cm}^{-1}$ . Powder X-ray diffraction (PXRD) patterns were measured with a Siemens  
129 D5000 apparatus using the  $\text{CuK}\alpha$  radiation. Patterns were recorded from  $2\theta = 5$  to  $50^\circ$ , with a step scan  
130 of  $0.02^\circ$  counting for 1 s at each step. Magnetic measurements from 5 to 300 K were carried out with a  
131 Quantum Design MPMS-5S SQUID susceptometer using a 100 Oe field.

132

### 133 Synthesis procedures

134  $[\text{Cu}(\mu\text{-pOHcinn})_2(4\text{-tBupy})_2(\text{H}_2\text{O})][\text{Cu}(\mu\text{-pOHcinn})_2(4\text{-tBupy})_2(\text{H}_2\text{O})_2]$  (1). A green solution of  
135  $\text{Cu}(\text{Ac})_2 \cdot \text{H}_2\text{O}$  (63 mg, 0.316 mmol) in MeOH (20 mL) was added to a solution containing HpOHcinn  
136 (104 mg, 0.632 mmol) and 4-tBupy (182 mg, 1.35 mmol) in MeOH (20 mL). The resulting green  
137 solution was concentrated up to 10 mL. Thus, a blue crystalline solid was formed, which was filtered  
138 and washed twice with 5 mL of cold MeOH and finally dried in the air. Yield: 120 mg (55.2%, respect  
139 to  $\text{Cu}(\text{Ac})_2 \cdot \text{H}_2\text{O}$ ). EA % calc. For  $\text{C}_{36}\text{H}_{43}\text{N}_2\text{O}_{7.5}\text{Cu}$  (687.29): C 62.91, H 6.31, N 4.08. Found: C  
140 62.63, H 6.35, N 4.09. ATR-FTIR (wavenumber,  $\text{cm}^{-1}$ ): 3156m  $\nu(\text{OH})_{\text{ar}}$ , 3014w  $\nu(\text{CH})_{\text{ar}}$ , 2967w  
141  $\nu(\text{CH})_{\text{al}}$ , 1634w, 1607m  $\nu(\text{COO}^-)$ , 1585w  $\nu(\text{CvC/CvN})_{\text{ar}}$ , 1531m, 1511s, 1438w  $\delta(\text{CvC/CvN})_{\text{ar}}$ ,  
142 1421w, 1387s  $\nu(\text{COO}^-)$ , 1277s, 1220s  $\delta(\text{OH})$ , 1167s, 1071m  $\delta(\text{C-H})_{\text{ar}}$ , ip, 1033w, 983s, 876w, 828s  
143  $\delta(\text{C-H})_{\text{ar}}$ , oop, 758m  $\delta(\text{C-H})_{\text{ar}}$ , oop, 684br.

144  $[\text{Cu}(\mu\text{-pOHcinn})_2(4\text{-Acpy})_2]_n$  (2). A green solution of  $\text{Cu}(\text{Ac})_2 \cdot \text{H}_2\text{O}$  (74 mg, 0.371 mmol) in MeOH  
145 (20 mL) was added to a solution of HpOHcinn (124 mg, 0.761 mmol) and 4-Acpy (201 mg, 1.66 mmol)  
146 in MeOH (20 mL). The resulting green solution was concentrated up to 15 mL. Thus, a dark blue  
147 crystalline solid was formed, which was filtered, washed with 5 mL of cold MeOH and finally dried in  
148 air. Yield: 186 mg (79.3%, respect to  $\text{Cu}(\text{Ac})_2 \cdot \text{H}_2\text{O}$ ). EA % calc. for  $\text{C}_{32}\text{H}_{28}\text{N}_2\text{O}_8\text{Cu}$  (632.10): C  
149 60.80; H 4.46; N 4.43. Found C 60.71; H 4.57; N 4.30. ATR-FTIR (wavenumber,  $\text{cm}^{-1}$ ): 3033  $\nu(\text{C-}$   
150  $\text{H})_{\text{ar}}$ ; 2981  $\nu(\text{C-H})_{\text{al}}$ , 1700  $\nu(\text{CvO})$ , 1635m, 1603s  $\nu(\text{COO}^-)$ , 1534s  $\nu(\text{CvC/CvN})_{\text{ar}}$ , 1508s, 1441w  
151  $\delta(\text{CvC/CvN})_{\text{ar}}$ , 1414s, 1385s  $\nu(\text{COO}^-)$ , 1355s, 1290w, 1258s, 1213s, 1168s, 1104w, 1058m  $\delta(\text{C-H})_{\text{ar}}$ ,  
152 ip, 1025w, 841s, 817s  $\delta(\text{C-H})_{\text{ar}}$ , oop, 724s  $\delta(\text{C-H})_{\text{ar}}$ , oop.

153  $\{[\text{Cu}(\mu\text{-pOHcinn})_2(3\text{-Phpy})_2] \cdot 2\text{MeOH}\}_n$  (3). A solution of  $\text{Cu}(\text{Ac})_2 \cdot \text{H}_2\text{O}$  (82 mg, 0.410 mmol) in  
154 MeOH (20 mL) was added to a solution of HpOHcinn (139 mg, 0.847 mmol) and 3-Phpy (252 mg, 1.62  
155 mmol) in MeOH 20 mL. The resultant green solution was concentrated up to 10 mL. Thus, a blue  
156 crystalline solid was formed, which was filtered, washed with 5 mL of cold MeOH and finally dried in  
157 air. The stoichiometry of this compound was definitively established after resolution of their X-ray  
158 crystal structure. However, this compound interchanges MeOH for water after being removed from the  
159 solution. Therefore, the manipulation required to prepare the sample for EA unavoidably led to a  
160 practically complete interchange. EA % calc. for  $\text{C}_{40}\text{H}_{36}\text{N}_2\text{O}_8\text{Cu}$  (736.27): C 65.52; H 4.40; N 3.80.  
161 Found C 65.21; H 4.38; N 3.84. After exposure to vacuum, trapped  $\text{H}_2\text{O}/\text{MeOH}$  is removed, leading to  
162  $[\text{Cu}(\mu\text{-pOHcinn})_2(3\text{-Phpy})_2]_n$ . EA % calc. for  $\text{C}_{40}\text{H}_{32}\text{N}_2\text{O}_6$  (700.14): C 68.61; H 4.61; N 4.00.  
163 Found: C 68.40; H 4.79; N 4.03. ATR-FTIR (as  $\{[\text{Cu}(\mu\text{-pOHcinn})_2(3\text{-Phpy})_2]_n \cdot 2\text{H}_2\text{O}\}_n$ , wavenumber,  
164  $\text{cm}^{-1}$ ): 3569w  $\nu(\text{O-H})_{\text{water}}$ , 3034w  $\nu(\text{C-H})_{\text{ar}}$ , 1632m, 1605m  $\nu(\text{COO}^-)$ , 1583m  $\nu(\text{CvC}/\text{CvN})_{\text{ar}}$ ,  
165 1529m, 1509s, 1478m, 1454m  $\delta(\text{CvC}/\text{CvN})_{\text{ar}}$ , 1374s  $\nu(\text{COO}^-)$ , 1288m, 1221s  $\delta(\text{OH})$ , 1168s, 1104w,  
166 1045m  $\delta(\text{C-H})_{\text{ar}}$ , ip, 990m, 934w, 875w, 832s  $\delta(\text{C-H})_{\text{ar}}$ , oop, 771s  $\delta(\text{C-H})_{\text{ar}}$ , oop, 751m, 695s  $\delta(\text{C-}$   
167  $\text{H})_{\text{ar}}$ , oop.  
168  $[\text{Cu}(\text{pOHcinn})_2(4\text{-Phpy})_2]_2[\text{Cu}(\text{pOHcinn})_2(4\text{-Phpy})_2] \cdot 1.5\text{MeOH} \cdot 2\text{H}_2\text{O}$  (4). A solution of  
169  $\text{Cu}(\text{Ac})_2 \cdot \text{H}_2\text{O}$  (120 mg, 0.601 mmol) in MeOH (20 mL) was added to a solution of HpOHcinn (210 mg,  
170 1.28 mmol) and 4-Phpy (394 mg, 2.54 mmol) in MeOH (20 mL). The resultant dark green solution was  
171 left in the fridge and protected from sunlight. After three hours, blue crystals precipitated. They were  
172 filtered and washed with 5 mL of MeOH and finally dried in the air, but always protected from sunlight.  
173 Yield: 196 mg (44.8% respect to  $\text{Cu}(\text{Ac})_2 \cdot \text{H}_2\text{O}$ ). EA % calc. for  $\text{C}_{121.50}\text{H}_{106}\text{N}_6\text{O}_{21.5}\text{Cu}_3$  (2184.81):  
174 C 66.79; H 4.89; N 3.85. Found C 66.75; H 4.67; N 3.85 ATR-FTIR (wavenumber,  $\text{cm}^{-1}$ ): 3014br  
175  $\nu(\text{OH})_{\text{ar}} + \nu(\text{CH})_{\text{ar}}$  1636m, 1606m  $\nu(\text{COO}^-)$ , 1585w  $\nu(\text{CvC}/\text{CvN})_{\text{ar}}$ , 1548m, 1509s, 1439m  
176  $\delta(\text{CvC}/\text{CvN})_{\text{ar}}$ , 1365br,  $\nu(\text{COO}^-)$ , 1237s  $\delta(\text{OH})$ , 1168s, 1072m  $\delta(\text{C-H})_{\text{ar}}$ , ip, 982w, 831s  $\delta(\text{C-H})_{\text{ar}}$ ,  
177 oop, 761s, 728m  $\delta(\text{C-H})_{\text{ar}}$ , oop, 689m  $\delta(\text{C-H})_{\text{ar}}$ , oop.  
178  $[\text{Cu}_2(\text{pOHcinn})_2(\text{trans-4-Phpy})_4(\mu\text{-pOcinn})_2\text{Cu}_2(\text{pOHcinn})_2(\text{cis-4-Phpy})_4]_n$  (5). This compound was  
179 prepared starting with the same reagents and solvent quantities that were used for compound 4, but  
180 putting the container under sunlight for a day. First, blue crystals were grown, which under sunlight  
181 slowly transformed into dark-blue crystals. Yield: 229 mg (62.2% respect to  $\text{Cu}(\text{Ac})_2 \cdot \text{H}_2\text{O}$ ). The  
182 compound 5 could also be obtained by suspending 4 in methanol and exposing the mixture to sunlight  
183 for a day. EA % calc. for  $\text{C}_{71}\text{H}_{56}\text{N}_4\text{O}_9\text{Cu}_2$  (1236.27): C 68.98; H 4.57; N 4.53. Found C 68.73; H  
184 4.59; N 4.53 ATR-FTIR (wavenumber,  $\text{cm}^{-1}$ ): 3013br  $\nu(\text{CH})_{\text{ar}}$ , 2931  $\nu(\text{C-H})_{\text{al}}$ ; 1635w, 1611m  
185  $\nu(\text{COO}^-)$ , 1591m  $\nu(\text{CvC}/\text{CvN})_{\text{ar}}$ , 1542s  $\nu(\text{COO}^-)$ , 1502s, 1447m  $\delta(\text{CvC}/\text{CvN})_{\text{ar}}$ , 1417w, 1386s  
186  $\nu(\text{COO}^-)$ , 1361s  $\nu(\text{COO}^-)$ , 1285s, 1235s  $\delta(\text{OH})$ , 1168s, 1102w, 1071w  $\delta(\text{C-H})_{\text{ar}}$ , ip, 1046w, 982m,  
187 862s, 831s  $\delta(\text{C-H})_{\text{ar}}$ , oop, 762s, 728s  $\delta(\text{C-H})_{\text{ar}}$ , oop, 689s  $\delta(\text{C-H})_{\text{ar}}$ , oop. The variation of the  
188 magnetization with temperature of 0.1052 g of 5 (0.085 mmol) in a 100 Oe field was measured. The

189 calculated diamagnetic contribution of this compound was found to be  $7.02 \times 10^{-4} \text{ cm}^3 \text{ mol}^{-1}$  using  
190 Pascal's constants.<sup>32</sup>

191

### 192 **X-ray crystal structures**

193 The X-ray intensity data were measured on a D8 Venture system equipped with a multilayer mono-  
194 chromate and a Mo microfocus ( $\lambda = 0.71073 \text{ \AA}$ ). For compounds 1–3, a blue prislake specimen was  
195 used for the X-ray crystallographic analysis. For compound 4, a blue needle specimen was used for the  
196 X-ray crystallographic analysis. For compound 5, a translucent blue-green specimen was used for the X-  
197 ray crystallographic analysis. Frames were integrated with the Bruker SAINT Software package using a  
198 narrow-frame algorithm. The structures were solved using the Bruker SHELXTL Software, packaged  
199 and refined using SHELXL (version-2018/3).<sup>33</sup> Data were corrected for absorption effects using the  
200 multi-scan method (SADABS, version 2008/1). Crystal data and additional details of structure  
201 refinement for compounds 1–5 are included in the ESI (Tables S1 and S2†). Molecular graphics were  
202 generated with the program Mercury 3.9.<sup>34,35</sup> Color codes for all molecular graphics are: orange (Cu),  
203 blue (N), red (O), grey (C), white (H).

204 The crystal quality of compound 4 was poor but an X-ray diffraction analysis was carried out, which  
205 clearly revealed the structure of the complex.

206

## 207 RESULTS AND DISCUSSION

208

### 209 Synthesis and general characterization

210 The reaction of copper acetate monohydrate ( $\text{Cu}(\text{Ac})_2 \cdot \text{H}_2\text{O}$ ) with (E)-3-(4-hydroxyphenyl)-2-propenoic  
211 acid (p-hydroxycinnamic acid, HpOHcinn) and different pyridine derivatives (dPy = 4-tBupy, 4-Acpy,  
212 3-Phpy, 4-Phpy) was essayed using MeOH as solvent with a molar ratio of 1 : 2 : 4 for Cu : HpOHcinn :  
213 dPy, and at room temperature and atmospheric pressure. Pyridine derivatives were added in excess to  
214 neutralize the MeCOOH byproduct. The tested reactions yielded four different compounds:  $[\text{Cu}(\mu\text{-}$   
215  $\text{pOHcinn})_2(4\text{-tBupy})_2(\text{H}_2\text{O})][\text{Cu}(\mu\text{-pOHcinn})_2(4\text{-tBupy})_2(\text{H}_2\text{O})_2]$  (1),  $[\text{Cu}(\mu\text{-pOHcinn})_2(4\text{-Acpy})_2]_n$   
216 (2),  $\{[\text{Cu}(\mu\text{-pOHcinn})_2(3\text{-Phpy})_2]_n \cdot 2\text{MeOH}\}_n$  (3) and  $[\text{Cu}(\text{pOHcinn})_2(4\text{-Phpy})_2]_2[\text{Cu}(\text{pOHcinn})_2(4\text{-}$   
217  $\text{Phpy})_2] \cdot 1.5\text{MeOH} \cdot 2\text{H}_2\text{O}$  (4) (Scheme 1). When a suspension of 4 in its mother liquor is exposed to  
218 sunlight, compound  $[\text{Cu}_2(\text{pOHcinn})_2(\text{trans-4-Phpy})_4(\mu\text{-p-Ocinn})_2\text{Cu}_2(\text{cis-4-Phpy})_4]_n$  (5) is obtained  
219 (Scheme 2), in which the phenol groups of half of the initial pOHCinn are deprotonated. Photoinduced  
220 intermolecular excited-state proton transfer (ESPT) reactions are ubiquitous in chemistry and  
221 biology.<sup>36,37</sup> Ligands that contain a proton donating group are also prone to be involved in these  
222 processes, since an additional excited state perturbation can occur where the electron density shift,  
223 associated with light absorption, significantly influences the acidity of the ligand.<sup>16,38</sup> Phenols are  
224 expected to be more acidic in the excited state than in the ground state.<sup>39,40</sup>

225 Products 1–5 were characterized via PXRD, Elemental Analyses (EA), ATR-FTIR spectroscopy and  
226 single crystal X-ray diffraction. Phase purity of the bulk samples for compounds 1, 2, 4 and 5 was  
227 confirmed via PXRD (ESI: Fig. S1–S4†). Compound 3, however, suffers a structural change when  
228 exposed to an open atmosphere; therefore, its PXRD patterns only match the one calculated from the  
229 solved structure when the sample is maintained under methanol vapors (see below). Again, EA data  
230 were also consistent with the elucidated single crystal X-ray structures of studied compounds, except for  
231 3. ATR-FTIR spectra of the five compounds confirm the presence of the organic ligands used in the  
232 synthesis, including bands assignable to dPy and pOHcinn anion (ESI: Fig. S5–S9†). The region  
233 between 3500 and 3000  $\text{cm}^{-1}$  shows several broad bands due the presence of  $\nu(\text{OH})$  and  $\nu(\text{CH})$ ar bands,  
234 hindering the possibility of extracting information on the role of the phenol group. However, in 3 (ESI:  
235 Fig. S10†) the disappearance of the band at 3396  $\text{cm}^{-1}$  and the formation of a band at 3570  $\text{cm}^{-1}$  were  
236 observed, which is consistent with the substitution of MeOH for H<sub>2</sub>O molecules in this compound.

237 Bands assignable to carboxylate groups provide key information about their coordination mode.<sup>41,42</sup>  
238 The difference measured between  $\nu_{\text{as}}(\text{COO}^-)$  and  $\nu_{\text{s}}(\text{COO}^-)$  is in the range of  $\Delta = 218 \text{ cm}^{-1}$ –233  
239  $\text{cm}^{-1}$  for 1–5, indicating a monodentate coordination mode.<sup>41</sup> In 4 and 5, other bands attributable to  
240  $\nu_{\text{as}}(\text{COO}^-)$  and  $\nu_{\text{s}}(\text{COO}^-)$  appear, possibly indicating other coordination modes.

241

242

243



## 244 **Molecular and extended structure**

245 It was possible to obtain single crystals for all reported compounds. In most of the cases, they were  
246 obtained from the initial reaction mixture after partial solvent evaporation (1–3), or by cooling the  
247 solution in the fridge (4). Single crystals of 5 were obtained from a suspension of 4 in methanol under  
248 sunlight. All of them were of good quality, allowing the elucidation of the X-ray crystal structure. The  
249 obtained crystal structures of 1–5 show great flexibility in the coordination mode of the pOHcinn ligand  
250 (Scheme 3), which leads to the formation of monomers, dimers and polymers with different  
251 coordination environments and geometries.

252 Compound 1. X-ray analysis reveals that compound 1 crystallizes in the monoclinic system with a  $C2/c$   
253 space group. 1 contains two crystallographic independent monomers in its unit cell:  $[\text{Cu}(\text{pOHcinn})_2(4\text{-}$   
254  $\text{tBupy})_2(\text{H}_2\text{O})_2]$  (1A) and  $[\text{Cu}(\text{pOHcinn})_2(4\text{-tBupy})_2(\text{H}_2\text{O})]$  (1B) (Fig. 1A). In each monomer, the  
255 Cu(II) cation is linked to two pOHcinn and two 4-tBupy ligands. The main difference is the number of  
256 coordinated H<sub>2</sub>O molecules, two in 1A and only one in 1B. Therefore, monomer 1A presents a  
257  $[\text{CuO}_4\text{N}_2]$  core with a distorted octahedral geometry, with two nitrogen atoms provided by two different  
258 4-tBupy, two oxygen atoms provided by two monodentate pOHcinn ligands and two oxygen atoms  
259 provided by two coordinated H<sub>2</sub>O molecules. Monomer 1B, having only one water, presents a square  
260 pyramidal geometry ( $\tau = 0.0245$ ),<sup>43</sup> with a  $[\text{CuO}_3\text{N}_2]$  core, with two nitrogen atoms provided by two  
261 different 4-tBupy, two oxygen atoms provided by two monodentate pOHcinn ligands and an oxygen  
262 atom provided by a coordinated H<sub>2</sub>O molecule.

263 For 1A, the basal plane is defined by two trans-coordinate 4-tBupy (Cu1A–N1B 2.019(3) Å) and two  
264 trans-coordinate monodentate pOHcinn moieties (Cu1A–O1A 1.982(3) Å). The apical positions are  
265 occupied by two weakly coordinating H<sub>2</sub>O molecules (Cu1A–O4A 2.440(3) Å). Bond angles are in the  
266 range of 85.12(9)–94.88(9)°. For 1B, 4-tBupy and pOHcinn ligands form the basal plane (Cu1B–N1B  
267 2.005(3) Å, Cu1B–O1B 1.968(2) Å) and the H<sub>2</sub>O ligand lies in the apical position (Cu1B–O4B 2.208(4)  
268 Å). The bond angles lie in the range of 87.83(12)–94.82(9)° and in the range of 170.36(17)°–  
269 171.74(15)°. All these distances and angles are in good agreement with related Cu(II) carboxylate-  
270 pyridine compounds.<sup>14,44,45</sup> Relevant distances and angles are summarized in Table 1.

271 The presence of two different monomeric units results in a supramolecular structure dominated by two  
272 distinct motifs: two different supramolecular 1-D chains along the b axis. Each chain is formed  
273 exclusively by the linkage via H-bonds of similar monomeric units; that is, a chain containing only 1A  
274 subunits and a different chain containing only 1B subunits. Similar motifs have been reported before in  
275 our group and in the literature.<sup>44,46</sup> Each monomer 1A has a symmetric quadruple H-bond, involving  
276 the coordinated O1A from the pOHcinn ligand and H4AB of the coordinated H<sub>2</sub>O molecule (Fig. 1B).  
277 Monomer 1B, on the other hand, forms an asymmetric double H-bond. In this monomer, the involved  
278 O2B is the uncoordinated oxygen from the pOHcinn ligand and H4BA of the coordinated H<sub>2</sub>O molecule  
279 (Fig. 1B). Other interesting distances are between intrachain and interchain Cu(II), which are  
280 Cu1A...Cu1A 5.999 Å, Cu1B...Cu1B 5.999 Å and Cu1A...Cu1B 14.137 Å. Compared to similar 1D

281 chain like structures, the interchain Cu...Cu distance is shorter when the carboxylate group belongs to  
282 acetate (around 8.2 Å)<sup>44,46</sup> or cinnamate (13.091 Å).<sup>45</sup> These chains are held together due to the role  
283 of the pOHcinn ligand. Its uncoordinated oxygen atoms of the carboxylate groups (O2A and O2B) form  
284 H-bonds with the –OH groups (H3AO and H3BO) of the different monomer. Thus, each monomer 1A is  
285 linked to four monomers 1B via the interaction of O2A with H3BO and each monomer 1B is linked to  
286 four monomers 1A via the interaction of O2B with H3AO (Fig. 1C). It is noteworthy that O2B also  
287 participates in the H-bonding of the proper B chain, thus playing a central structural role. Relevant H-  
288 bond interactions are summarized in Table 2.

289 Compounds 2 and 3. X-ray analysis reveals that 2 and 3 crystallize in a monoclinic system with a P21/n  
290 space group. Both show similar 2D-polymeric structures: [Cu(μ-pOHcinn)<sub>2</sub>(4-Acpy)<sub>2</sub>]<sub>n</sub> (2) and {[Cu(μ-  
291 pOHcinn)<sub>2</sub>(3-Phpy)<sub>2</sub>·2MeOH]<sub>n</sub> (3) (Fig. 2A), in which the pOHcinn ligand acts as a ditopic  
292 bimonodentate bridge. Due to its similarity, they are here described together. In both, each repeating  
293 unit consists of an octahedral [CuO<sub>4</sub>N<sub>2</sub>] core.

294 Their basal plane is defined by two of the oxygen atoms provided by the carboxylate groups of two  
295 different pOHcinn ligands coordinating in a monodentate fashion (Cu–O1 1.9280(9) Å for 2 and  
296 1.9640(12) Å for 3) and two nitrogen atoms corresponding to two pyridine ligands (4-Acpy) (2) or 3-  
297 Phpy (3) (Cu–N1 2.0521(11) Å for 2 and 1.9975(14) Å for 3). The apical positions are occupied by two  
298 phenolic groups from two different pOHcinn ligands (Cu–O3 2.5951(12) Å in 2 and 2.4925(13) in 3).  
299 Bond angles are in the range of 82.88(4)°–91.73(4)° for 2 and 89.07(5)°–95.05(6)° for 3. Relevant  
300 distances and angles for 2 and 3 are summarized in Table 3. The four pOHcinn anions bridge the four  
301 closer copper atoms in the (101) plane (2) or (12 0 12) (3) acting as a ditopic bis-monodentate bridging  
302 ligand (Scheme 3) via one oxygen from the carboxylate group and one oxygen of the phenol  
303 functionality, both from pOHcinn, forming 2D polymeric layers. Therefore, each pOHcinn ligand is  
304 shared by two metal centers. This configuration has also been reported in the [Cu(pOHBz)<sub>2</sub>(4-Bzpy)<sub>2</sub>]<sub>n</sub>  
305 polymer with similar distances, except the Cu–Ophenol distance (2.7449(19) Å), which is longer than  
306 that in either 2 and 3.<sup>14</sup> For 2 and 3, the uncoordinated oxygen O2 forms an intramolecular H-bond  
307 H3A, which is the hydrogen of the phenol group of an adjacent pOHcinn ligand (Fig. 2A and B). This  
308 hydrogen bond defines a sort of 6-member ring [Cu–O1–C1–O2...H3–O3] reinforcing the layered  
309 structure. In 3, O2 also forms a second weaker hydrogen bond with a MeOH molecule.

310 For 2 and 3 compounds, each monomer is linked to four other monomers, defining 2D-layers (Fig. 2B).  
311 The Cu(O1)<sub>2</sub>(N1)<sub>2</sub> plane tilts 67.51° in 2 and 87.25° in 3 with respect to each other and in alternate  
312 fashion for each bonded monomer, while the carboxylate groups (O1–C1–O2) from the pOHcinn are  
313 almost coplanar with their benzene rings (8.13° in 2 and 19.66° in 3). This arrangement results in  
314 pOHcinn bridges being situated closer to the mean plane defined by the Cu(II) ions, while 4-Acpy or 3-  
315 Pypy ligands stand out, enabling them to interleave with pyridine derived ligands of the neighboring 2D  
316 layers (Fig. 3A). This supramolecular arrangement is similar to the one found in [Cu(μ-pOHBz)<sub>2</sub>(4-  
317 Phpy)<sub>2</sub>] and [Cu(μ-pOHBz)<sub>2</sub>(4-Bzpy)<sub>2</sub>]<sub>n</sub>.<sup>14</sup> This allows the formation of H-bonds that hold the layers

318 together in a 3D supramolecular structure. In 2, the carbonyl group of 4-Acpy is responsible for these  
319 interaction, forming an H-bond with the hydrogen on the para position of the neighboring 4-Acpy  
320 ligand. In 3, a different supramolecular force is holding the layers together; an H- $\pi$  bonding between  
321 H12 of the 3-Phpy and the benzene ring of the pOHcinn ligand (Fig. 3B). Relevant H-bond interactions  
322 are summarized in Table 4.

323 Compound 2 shows a compact packing, facilitated by the orientation of the 4-Acpy ligand with respect  
324 to the 2D network. On the contrary, in 3, the larger size of the 3-Phpy ligand results in the phenyl  
325 substituents being orientated outwards, leaving tridimensional elongated cavities filled with MeOH  
326 molecules. These cavities are connected through choke points defining zig-zag channels (Fig. 4A).  
327 These channels occupy a total volume of approximately 10.6% (197.99 Å<sup>3</sup>, calculated using a probe  
328 radius of 1.2 Å).<sup>47</sup> This different behaviour can be related to the shape of the auxiliary pyridine ligands  
329 preventing close packing of the layers, as 4-Acpy results in an interlayer Cu $\cdots$ Cu distance of 8.434 Å  
330 (2), whereas for 3-Phpy this distance is 15.201 Å (3). Furthermore, the free space in 3 is much larger  
331 than the reported 4.2% for the [Cu( $\mu$ -pOHBz)<sub>2</sub>(4-Bzpy)<sub>2</sub>]<sub>n</sub> polymer.<sup>14</sup> However, this result shows that  
332 not only a longer spacer between the phenol and the carboxylate functional groups is required for  
333 increasing the free space, but also functional groups that prevent the stacking of the layers from  
334 obstructing the cavities.

335 When exposed to air, the compound changes from dark blue crystals to pale blue powder. Furthermore,  
336 XRD analyses reveal that this process is accompanied by a structural change (Fig. 4B). FTIR-ATR  
337 spectra also confirm this structural change (ESI: Fig. S10<sup>†</sup>). EA of the pale blue powder suggests that  
338 MeOH molecules are substituted by two H<sub>2</sub>O molecules. Therefore, a MeOH–H<sub>2</sub>O exchange process  
339 occurs, in spite of the choke point, evidencing some structure flexibility. PXRD analysis shows that the  
340 process can be reversed by exposing the powdered sample to a MeOH saturated atmosphere, exchanging  
341 H<sub>2</sub>O molecules for MeOH molecules. The XRD pattern of the sample in contact with methanol vapors  
342 matches the simulated from the crystal structure data (Fig. 4). Therefore, it is clear that compound 3 is a  
343 2D-MOF, which interchange water and methanol molecules in a reversible manner. However, trials to  
344 measure the specific surface area by studying N<sub>2</sub> adsorption–desorption failed due to the collapse of the  
345 structure during the degasification step. EA performed after vacuum exposure confirms that all solvent  
346 molecules have been removed. This suggests that solvent molecules are necessary to stabilize the porous  
347 supramolecular net, and that full removal of the solvents causes irreversible collapse of the channels.  
348 PXRD performed after vacuum exposure denotes that a different structure is formed (Fig. 4B).

349 Compound 4. This compound crystallizes in the triclinic system with a P1<sup>-</sup> space group and has a  
350 complex structure containing two crystallographic independent units, a dimer [Cu(pOHcinn)<sub>2</sub>(4-  
351 Phpy)<sub>2</sub>]<sub>2</sub> (4A) and a monomer [Cu(pOHcinn)<sub>2</sub>(4-Phpy)<sub>2</sub>] (4B) and included solvent molecules (Fig.  
352 5A).

353 Dimer 4A shows Cu(II) cations with a slightly distorted square pyramidal coordination geometry ( $\tau =$   
354 0.028)<sup>43</sup> and a [CuO<sub>3</sub>N<sub>2</sub>] core with the three oxygen atoms provided by three carboxylate groups from

355 different pOHcinn ligands and two nitrogen atoms provided by two different 4-Phpy ligands. The basal  
356 plane is defined by one pOHcinn acting as a monodentate ligand (Cu1–O1 1.937(4) Å), another  
357 pOHcinn acting as a ditopic bis-monodentate bridged ligand (Cu–O3 1.967(3) Å) and the two nitrogen  
358 atoms of the 4-Phpy ligands (Cu1–N1 2.016(4) Å, Cu1–N2 2.002(4) Å). The apical position is occupied  
359 by one oxygen of a pOHcinn acting as a ditopic bis-monodentate bridging ligand (Cu1–O3#1 2.378(3)  
360 Å) (Scheme 3). The Cu···Cu separation is 3.417 Å. The bond angles are in the range of 76.70(13)°–  
361 94.87(15)° and 171.17(17)°–172.88(16)°. The smallest bond angle of 76.70(13)° is due to the rigid  
362 nature of the Cu1–O3–Cu1–O3 ring. The morphology of this compound is notably similar to the closely  
363 related [Cu(cinn)<sub>2</sub>(β-pic)<sub>2</sub>] compound (cinn = cinnamate, β-pic = β-picoline) described in the  
364 literature.<sup>34</sup> The bond lengths and angles are in the range of similar compounds.<sup>45,48–50</sup>

365 Monomer 4B, on the other hand, presents a square planar geometry with a [CuO<sub>2</sub>N<sub>2</sub>] core, with two  
366 monodentate pOHcinn and two 4-Phpy ligands in trans positions (Cu<sub>2</sub>–O7 1.934(4) Å, Cu<sub>2</sub>–N3  
367 2.004(4)). The bond angles are in the range of 89.52(17)°–90.48(17)°. Relevant distances and angles are  
368 provided in Table 5.

369 The presence of occluded solvent molecules (MeOH and H<sub>2</sub>O), non-coordinating oxygen atoms of  
370 carboxylate from monodentate pOHcinn ligands and phenolic alcohols allows for the formation of 2D  
371 supramolecular layers. These layers can be described as alternating parallel threads of dimers 4A and  
372 monomers 4B (Fig. 5B). Each dimer interacts with two similar dimers due to the mediation of four H<sub>2</sub>O  
373 molecules, forming a symmetric double bridge. This double bridge involves a phenolic OH group (O5–  
374 H5O···O4 W) and a free oxygen of a monodentate pOHcinn (O4W–H4WB···O4, Fig. 6A).

375 Furthermore, each dimer interacts with two monomers, via a non-coordinating oxygen of the  
376 carboxylate from a monodentate pOHcinn ligand of the monomer and the remaining phenolic hydrogen  
377 (O6–H6O···O8) and another free oxygen of a monodentate pOHcinn ligand of the dimer and the  
378 remaining phenolic hydrogen of the monomer (O9–H9O···O2) (Fig. 6B). The intralayer Cu1···Cu2  
379 distance is 10.563 Å, whereas the interlayer Cu1···Cu1 and Cu2···Cu2 distance is 12.956 Å. Relevant H-  
380 bond interactions are summarized in Table 6. The fact that in this compound solvent molecules occupy  
381 non interconnected cavities (12.9%, 370.42 Å<sup>3</sup>, using a probe radius of 1.2 Å)<sup>47</sup> (Fig. 7) explains its  
382 stability compared with compound 3.

383 Compound 5. When a methanolic suspension of 4 is exposed to sunlight, it is transformed into  
384 compound [Cu<sub>2</sub>(pOHcinn)<sub>2</sub>(trans-4-Phpy)<sub>4</sub>(μ-pOcinn)<sub>2</sub>Cu<sub>2</sub>(pOHcinn)<sub>2</sub>(cis-4-Phpy)<sub>4</sub>]<sub>n</sub> (5). Further  
385 testing reveals that this result is not achieved by heating the same methanolic suspension or exposing it  
386 to UV light. Single crystal X-ray analyses reveal that 5 crystallizes in the monoclinic system with a  
387 C<sub>2</sub>/C space group. Compound 5 consists of a polymeric 1D-chain formed by two different Cu(II)  
388 dimeric subunits, named 5-cis and 5-trans, respectively, according to the relative position of the 4-Phpy  
389 ligands. The polymer shows a [5-trans-(μ-pOcinn)-5-cis-(μ-pOcinn)]<sub>n</sub> concatenation (Fig. 8), with the  
390 bridging μ-pOcinn linkers shared by the two subunits. In 5-trans μ-pOcinn coordinates through the  
391 carboxylate group while in 5-cis coordinates through the phenoxy groups. Both subunits have a penta-

392 coordinated [CuO<sub>3</sub>N<sub>2</sub>] core, but their topology and conformation are radically different. In subunit 5-  
393 trans, Cu(II) cations have a slightly distorted square pyramidal ( $\tau = 0.0245$ )<sup>43</sup> geometry, comprising two  
394 oxygen atoms in the basal plane (Cu1–O1 1.9755(15) Å and Cu1–O4 1.9365(15) Å), the first provided  
395 by the carboxylate group of the pOHcinn moiety and the second by the carboxylate group of the  $\mu$ -  
396 pOcinn ligand, and two nitrogen atoms (Cu1–N1 2.0166(19) Å, Cu1–N2 2.0246(19) Å) of the two 4-  
397 Phpy. The apical position is occupied by an oxygen of another pOcinn ligand (Cu1–O1# 2.3438(16) Å).  
398 The subunit shows the versatility of the coordination modes of the coumaric acid. Cu(II) is coordinated  
399 to three coumaric acids (two monodentate bridging (pOHcinn) and one ditopic bis-monodentate bridge  
400 ( $\mu$ -pOcinn)) linking the subunit 5-trans with the subunit 5-cis.

401 In subunit 5-cis, the two Cu(II) cations are also pentacoordinated, with the pyridines being in a cis  
402 position. Thus, the coordination geometry is a distorted square pyramid ( $\tau = 0.343$ )<sup>43</sup>. The basal plane is  
403 formed by one phenol oxygen of the linking pOcinn ligand bridging two Cu(II) atoms (Cu2–O6  
404 1.9402(15) Å), one oxygen of a carboxylate from the monodentate pOHcinn ligand (Cu2–O7 2.0016(15)  
405 Å) and two nitrogen atoms of two 4-Phpy (Cu2–N3 2.0484(19) Å, Cu2–N4 1.9975(18) Å). The apical  
406 position is occupied by another phenol oxygen of the linking pOcinn ligand bridging two Cu(II) atoms  
407 (Cu2–O6 1.9402(15) and Cu2–O6#1 2.2521(15) Å). Relevant distances and angles are summarized in  
408 Table 7.

409 To summarize the differences between the two subunits, it is worth remarking the following: the most  
410 important of them is the fact that in subunit 5-trans all oxygen atoms are of the carboxylic groups of the  
411 pOHcinn ligand, whereas in subunit 5-cis they coordinate via carboxylic and phenolate groups.

412 Furthermore, the relative position of their ligands is also different. Subunit 5-trans has a trans  
413 configuration, forming a sort of flat Cu1–O1–Cu1–O1 4-member ring with 4-Phpy and having pOHcinn  
414 ligands perpendicular ( $89.27^\circ$ ) and parallel ( $12.44^\circ$ ) to it, respectively, and a Cu1...Cu1 distance of  
415 3.389 Å.

416 The subunit 5-cis, although maintaining pOcinn ligands in the trans position, has the 4-Phpy ligands in  
417 the cis position (their pyridine rings defining a  $96.99^\circ$  angle between their centroids) and pOHcinn  
418 ligands acting as monodentate are also in cis positions. The Cu2–O6–Cu2–O6 ring has a V-like shape  
419 with a shorter Cu2...Cu2 distance of 3.013 Å. The two dimers lie at an intrachain Cu1...Cu2 distance of  
420 11.470 Å.

421 The resulting 1-D polymeric structure could be described as a block copolymer with an ABAB  
422 configuration. These chains run along the (12 0 12) direction with an S-like shape. These chains are  
423 stacked in parallel via an interaction between a noncoordinated phenolic hydrogen and a free oxygen of  
424 a carboxylic acid (O9–H9A...O5), forming a 3D supramolecular structure. This supramolecular structure  
425 is further reinforced via weaker double C–H...O interactions (C41–H41...O1 and C42–H42...O1)  
426 involving hydrogen atoms in the pyridine ring of 4-Phpy and oxygen atoms of the carboxylate groups  
427 (Fig. 9). This arrangement results in an interchain Cu...Cu distance of 14.436 Å. Relevant  
428 supramolecular forces are summarized in Table 8.

429 Magneto-structural correlations in compound 5. The 1D polymeric chains of 5 contain two dimers with  
430 different active magnetic exchange pathways, one corresponding to 5-trans, where we can find  
431 carboxylate monodentate bridges, and the other being 5-cis where the bridges are formed via onodentate  
432 phenoxy moieties. The value of  $\chi_p T$  decreases upon cooling up to 30 K, where a small plateau-like  
433 region appears. This trend of small  $\chi_p T$  decrease ended at around 7 K, when another steeper decrease  
434 region is resumed (Fig. 10), suggesting an antiferromagnetic behavior.

435 In the first approximation, Cu(II) coupling through the pOcinn ligand was assumed negligible (shortest  
436 interdimer distance 11.866 Å). Therefore, the magnetic behavior of 5 must be considered as the addition  
437 of two independent dimers using a slightly modified Bleany–Bowers equation.<sup>50,51</sup> The adjustment  
438 yielded a negligible  $\rho$  value of 0.01%. Therefore, this term was removed for the sake of simplification.

439 The resulting equation was:

440

$$\chi_{\text{para}} = \frac{2 \cdot N g^2 \cdot \beta^2}{K \cdot T \cdot \left[ 3 + e^{\frac{-J}{kT}} \right]} + \frac{2 \cdot N g^2 \cdot \beta^2}{K \cdot T \cdot \left[ 3 + e^{\frac{-J}{kT}} \right]}$$

441

442

443 The model reproduces satisfactorily the magnetic properties in the range of 0 to 303 K with the  
444 parameters ( $g = 2.16$ ;  $J_1(\text{cm}^{-1}) = -75.10$ ;  $J_2(\text{cm}^{-1}) = -1.74$ ;  $H = -J_{\text{SiSi}+1}$ ).

445 It has been known since longtime that Cu(II) dimers bridged by double phenoxy groups show a great  
446 variability of J values ranging from ferromagnetic to strong antiferromagnetic.<sup>52</sup> This variability has  
447 prompted a strong debate about which are the magneto-structural correlations. The consensus is that five  
448 of them are key: the Cu...Cu distance, Cu–O–Cu angle, Cu–O distance, dihedral angle between the two  
449 coordination planes and planarity of the bonds around the coordinating atom.<sup>52,53</sup> This is also applied  
450 in Cu(II) dimers bridged by phenoxy groups.<sup>54–56</sup> Most of the Cu<sub>2</sub>O<sub>2</sub> core magnetic pathways  
451 including phenolic oxygen atoms are antiferromagnetic,<sup>53,55–58</sup> but a few of them are ferromagnetic.

452 59 Taking this into account, the J<sub>1</sub> value could be assigned to the 5-cis subunit, as its value is in the  
453 range of other phenoxy-bridged Cu(II) dimers.<sup>59</sup> Its moderately antiferromagnetic interaction can be  
454 explained due the fact that the  $-2J$  value decreases with lower angles up to the crossover point of 77°. <sup>54</sup>  
455 However, this parameter alone cannot explain this weak interaction, as  $J = -75.10 \text{ cm}^{-1}$  is lower than  
456 expected with a Cu–O–Cu angle value of 91.57°. The weak antiferromagnetic interaction could also be  
457 due to the V shape of 5-cis, where O–Cu–O coordination planes having a dihedral angle of 51.24°. This  
458 morphology lowers the antiferromagnetic interaction due to the loss of orbital overlap.<sup>59</sup>

459 The other exchange magnetic pathway,  $J_2 = -1.74 \text{ cm}^{-1}$ , which also shows an antiferromagnetic  
460 interaction, has a Cu<sub>2</sub>O<sub>2</sub> core too, but including carboxylate bridges. Those pathways are well known  
461 and have been thoroughly studied.<sup>60</sup> However, in 5-trans the bridging oxygen atoms are not both in the  
462 equatorial plane; in fact, one is in the equatorial plane and the other in the apical position. Reports of this

463 combination for Cu(II) dimers are scarce and no general trends have been found yet.<sup>48–50</sup> However, the  
464 consensus is that, although these types of core can be ferromagnetic or antiferromagnetic, they always  
465 show a weak interaction which agrees with the reported values here.<sup>48–50</sup>

466

467

468 **CONCLUSION**

469

470 A family of five Cu(II) coordination compounds including HpOHcinn acid and pyridine derivatives, 4-  
471 tBupy, 4-Acpy, 3-Phpy and 4-Phpy, is presented here. The analysis of their crystal structures shows how  
472 the choice of the pyridine ligand determines different coordination modes of the pOHcinn ligand, as  
473 well as the Cu(II) coordination, nuclearity and geometry. The pOHcinn acts as a monodentate  
474 carboxylate ligand in 1 and 4, yielding monomers and dimers, and the phenol group playing a key role  
475 in the hydrogen bond networks that determined the extended structure of both compounds. In contrast,  
476 when pOHcinn acts as a ditopic ligand, it leads to the formation of 2D coordination polymers, as  
477 observed in 2 and 3. The increase of the distance between the phenol and the carboxylate functionalities  
478 in the pOHcinn ligand is significant, compared to that with the previously studied pOHBz ligand,  
479 resulting in an overall increase of the available empty space for certain compounds. Compound 3 shows  
480 promising results, as it exchanges MeOH for H<sub>2</sub>O and vice versa, when exposed to different  
481 atmospheres, suffering a structural change in the process. This exchange is reversible, although full  
482 removal of solvents gives a non-porous material. Besides the effect of the pyridine substituents on the  
483 coordination mode of pOHcinn, the choice of the pyridine also determines its susceptibility to undergo a  
484 photoinduced process. Probably due to an increase in the acidity of the phenol group, half of the  
485 pOHcinn ligands in 4 are deprotonated when exposed to sunlight, generating a dianionic ligand that also  
486 acts as a linker between metal centers, resulting in the formation of polymer 5. This coordination  
487 polymer behaves magnetically as the sum of two independent dimers, due to a long interdimer distance  
488 (11.866 Å). One of the dimers has a  $J_1$  value of  $-75.10 \text{ cm}^{-1}$  and is assigned to the 5-cis subunit. This  
489 value is somewhat lower than the reported values of similar dimers, which can be explained by other  
490 structural factors such as the shape and Cu...Cu distance. The other dimer has a value of  $J_2 = -1.74$   
491  $\text{cm}^{-1}$ . Compared to other monodentate carboxylate bridged dimers, this value is low. This can be  
492 explained by the structural particularity mentioned before, that is, the fact of having one bridge in an  
493 equatorial position and one bridge in the axial position.

494

495

496



497 **CONFLICTS OF INTEREST**

498 There are no conflicts to declare

499

500

501

502 **ACKNOWLEDGEMENTS**

503

504 .This work was partially financed by the Spanish National Plan of Research (projects CTQ2014-56324,  
505 CTQ2017-83632 and MAT2015-65756-R) and by the Generalitat de Catalunya (project 2014SGR377).  
506 C. D./ICMAB acknowledges financial support from the Spanish MEC, through the “Severo Ochoa”  
507 Programme for Centres of Excellence in R&D (SEV-2015-0496) J. S. also acknowledges the Universitat  
508 Autònoma de Barcelona for his pre-doctoral grant.

509

510 **REFERENCES**

511

512 1 M. E. Davis, *Nature*, 2002, 417, 813–821.

513 2 P. Silva, S. M. F. Vilela, J. P. C. Tomé and F. A. Almeida Paz, *Chem. Soc. Rev.*, 2015, 44,  
514 6774–6803.

515 3 G. Maurin, C. Serre, A. Cooper and G. Férey, *Chem. Soc. Rev.*, 2017, 46, 3104–3107.

516 4 Y. He, S. Xiang and B. Chen, *J. Am. Chem. Soc.*, 2011, 133, 14570–14573.

517 5 H. Wang, H. Wu, J. Kan, G. Chang, Z.-Z. Yao, B. Li, W. Zhou, S. Xiang, J. Cong-Gui Zhao and  
518 B. Chen, *J. Mater. Chem. A*, 2017, 5, 8292–8296.

519 6 A. Karmakar, R. Illathvalappil, B. Anothumakkool, A. Sen, P. Samanta, A. V. Desai, S.  
520 Kurungot and S. K. Ghosh, *Angew. Chem., Int. Ed.*, 2016, 55, 10667–10671.

521 7 F. Hu, C. Liu, M. Wu, J. Pang, F. Jiang, D. Yuan and M. Hong, *Angew. Chem., Int. Ed.*, 2017,  
522 56, 2101–2104.

523 8 W. Yang, J. Wang, H. Wang, Z. Bao, J. C.-G. Zhao and B. Chen, *Cryst. Growth Des.*, 2017, 17,  
524 6132–6137.

525 9 Z. Ju, G. Liu, Y.-S. Chen, D. Yuan and B. Chen, *Chem. – Eur. J.*, 2017, 23, 4774–4777.

526 10 H. Wahl, D. A. Haynes and T. le Roex, *Cryst. Growth Des.*, 2017, 17, 4377–4383.

527 11 R. P. Sharma, A. Singh, A. Saini, P. Venugopalan, A. Molinari and V. Ferretti, *J. Mol. Struct.*,  
528 2009, 923, 78–84.

529 12 S. Gomathi and P. T. Muthiah, *Acta Crystallogr., Sect. C: Cryst. Struct. Commun.*, 2013, 69,  
530 1498–1502.

531 13 F. Valach, M. Dunaj-Jurčo, M. Melnik and N. N. Hoang, *Z. Kristallogr.*, 1994, 209, 267–270.

532 14 M. Sanchez-Sala, J. Pons, Á. Álvarez-Larena, C. Doming and J. A. Ayllón, *ChemistrySelect*,  
533 2017, 2, 11574–11580.

534 15 K. F. White, B. F. Abrahams, R. Babarao, A. D. Dharma, T. A. Hudson, H. E. Maynard-Casely  
535 and R. Robson, *Chem. – Eur. J.*, 2015, 21, 18057–18061.

- 536 16 H. Görner, S. Khanra, T. Weyhermüller and P. Chaudhuri, *J. Phys. Chem. A*, 2006, 110, 2587–  
537 2594.
- 538 17 X.-Y. Fan, K. Li, X.-C. Huang, T. Sun, K.-T. Wang, R.-R. Yun and H.-L. Wu, *Z. Kristallogr. –*  
539 *New Cryst. Struct.*, 2009, 224, 59–61.
- 540 18 Y. Z. Jia-Yuan Mao, H.-X. Fang, Q.-F. Xu, Q.-X. Zhou and J.-M. Lu, *Chin. J. Inorg. Chem.*,  
541 2008, 24, 1046–1050.
- 542 19 H.-L. Wu, W.-K. Dong and X.-L. Wang, *Z. Kristallogr. – New Cryst. Struct.*, 2007, 222, 36–38.
- 543 20 X. Qing-Feng, Z. Qiu-Xuan, L. Jian-Mei, X. Xue-Wei and Z. Yong, *J. Solid State Chem.*, 2007,  
544 180, 207–212.
- 545 21 M. Kalinowska, L. Mazur, J. Piekut, Z. Rzączyńska, B. Laderiere and W. Lewandowski, *J.*  
546 *Coord. Chem.*, 2013, 66, 334–344.
- 547 22 L. Chen, *Z. Kristallogr. – New Cryst. Struct.*, 2009, 224, 565–566.
- 548 23 V. Zeleňák, I. Císařová and P. Llewellyn, *Inorg. Chem. Commun.*, 2007, 10, 27–32.
- 549 24 L. Chen, *Acta Crystallogr., Sect. E: Struct. Rep. Online*, 2009, 65, m807–m807.
- 550 25 G. B. Deacon, M. Forsyth, P. C. Junk, S. G. Leary and W. W. Lee, *Z. Anorg. Allg. Chem.*, 2009,  
551 635, 833–839.
- 552 26 H. Li and C. W. Hu, *J. Solid State Chem.*, 2004, 177, 4501–4507.
- 553 27 J. Yan, Y. Guo, H. Li, X. Sun and Z. Wang, *J. Mol. Struct.*, 2008, 891, 298–304.
- 554 28 A. Mukherjee, M. K. Saha, M. Nethaji and A. R. Chakravarty, *New J. Chem.*, 2005, 29, 596.
- 555 29 S. Gupta, A. Mukherjee, M. Nethaji and A. R. Chakravarty, *Polyhedron*, 2005, 24, 1922–1928.
- 556 30 H.-L. Wu, J.-G. Liu, P. Liu, W.-B. Lv, B. Qi and X.-K. Ma, *J. Coord. Chem.*, 2008, 61, 1027–  
557 1035.
- 558 31 A. Mukherjee, M. K. Saha, M. Nethaji and A. R. Chakravarty, *Chem. Commun.*, 2004, 475,  
559 716.
- 560 32 G. A. Bain and J. F. Berry, *J. Chem. Educ.*, 2008, 85, 532.
- 561 33 G. M. Sheldrick, *Acta Crystallogr., Sect. C: Cryst. Struct. Commun.*, 2015, 71, 3–8.

- 562 34 C. F. Macrae, I. J. Bruno, J. A. Chisholm, P. R. Edgington, P. McCabe, E. Pidcock, L.  
563 Rodriguez-Monge, R. Taylor, J. Van De Streek and P. A. Wood, *J. Appl. Crystallogr.*, 2008, 41,  
564 466–470.
- 565 35 C. F. Macrae, P. R. Edgington, P. McCabe, E. Pidcock, G. P. Shields, R. Taylor, M. Towler and  
566 J. Van De Streek, *J. Appl. Crystallogr.*, 2006, 39, 453–457.
- 567 36 P. K. Singh and A. Awasthi, *ChemPhysChem*, 2017, 198–207.
- 568 37 N. Agmon, *J. Phys. Chem. A*, 2005, 109, 13–35.
- 569 38 A. Das, T. Banerjee and K. Hanson, *Chem. Commun.*, 2016, 52, 1350–1353.
- 570 39 M. Kuss-Petermann and O. S. Wenger, *J. Phys. Chem. A*, 2013, 117, 5726–5733.
- 571 40 R. M. O'Donnell, R. N. Sampaio, G. Li, P. G. Johansson, C. L. Ward and G. J. Meyer, *J. Am.*  
572 *Chem. Soc.*, 2016, 138, 3891–3903.
- 573 41 G. Gliemann, *Ber. Bunsenges. Phys. Chem.*, 1978, 82, 1263–1263.
- 574 42 G. Deacon, *Coord. Chem. Rev.*, 1980, 33, 227–250.
- 575 43 A. W. Addison, T. N. Rao, J. Reedijk, J. van Rijn and G. C. Verschoor, *J. Chem. Soc., Dalton*  
576 *Trans.*, 1984, 1349–1356.
- 577 44 R. Kruszynski, A. Adamczyk, J. Radwańska-Doczekalska and T. Bartczak, *J. Coord. Chem.*,  
578 2002, 55, 1209–1217.
- 579 45 R. P. Sharma, A. Saini, P. Venugopalan, J. Jezierska and V. Ferretti, *Inorg. Chem. Commun.*,  
580 2012, 20, 209–213.
- 581 46 J. Soldevila-Sanmartín, J. A. Ayllón, T. Calvet, M. Font-Bardia and J. Pons, *Polyhedron*, 2017,  
582 135, 36–40.
- 583 47 A. L. Spek, *J. Appl. Crystallogr.*, 2003, 36, 7–13.
- 584 48 J. Pasán, J. Sanchiz, C. Ruiz-Pérez, F. Lloret and M. Julve, *New J. Chem.*, 2003, 27, 1557–1562.
- 585 49 R. Baldomá, M. Monfort, J. Ribas, X. Solans and M. A. Maestro, *Inorg. Chem.*, 2006, 45, 8144–  
586 8155.
- 587 50 R. Bikas, P. Aleshkevych, H. Hosseini-Monfared, J. Sanchiz, R. Szymczak and T. Lis, *Dalton*  
588 *Trans.*, 2015, 44, 1782–1789.

- 589 51 B. Bleaney and K. D. Bowers, *Proc. R. Soc. London, Ser. A*, 1952, 214, 451–465.
- 590 52 V. H. Crawford, H. W. Richardson, J. R. Wasson, D. J. Hodgson and W. E. Hatfield, *Inorg.*  
591 *Chem.*, 1976, 15, 2107–2110.
- 592 53 G. Dutta, R. K. Debnath, A. Kalita, P. Kumar, M. Sarma, R. B. Shankar and B. Mondal,  
593 *Polyhedron*, 2011, 30, 293–298.
- 594 54 L. K. Thompson, S. K. Mandal, S. S. Tandon, J. N. Bridson and M. K. Park, *Inorg. Chem.*,  
595 1996, 35, 3117–3125.
- 596 55 A. Biswas, M. G. B. Drew, J. Ribas, C. Diaz and A. Ghosh, *Eur. J. Inorg. Chem.*, 2011, 2405–  
597 2412.
- 598 56 A. Biswas, M. G. B. Drew, J. Ribas, C. Diaz and A. Ghosh, *Inorg. Chim. Acta*, 2011, 379, 28–  
599 33.
- 600 57 N. Novoa, F. Justaud, P. Hamon, T. Roisnel, O. Cador, B. Le Guennic, C. Manzur, D. Carrillo  
601 and J.-R. Hamon, *Polyhedron*, 2015, 86, 81–88.
- 602 58 Q. R. Cheng, H. Zhou, Z. Q. Pan, G. Y. Liao and Z. G. Xu, *Polyhedron*, 2014, 81, 668–674.
- 603 59 P. Chaudhuri, R. Wagner and T. Weyhermüller, *Inorg. Chem.*, 2007, 46, 5134–5136.
- 604 60 G. Psomas, C. P. Raptopoulou, L. Iordanidis, C. Dendrinou-Samara, V. Tangoulis and D. P.  
605 Kessissoglou, *Inorg. Chem.*, 2000, 39, 3042–3048.
- 606

607 **Legends to figures**

608

609 **Scheme 1.** Reactions carried out in this work. Isolated and characterized products are shown with their  
610 numbering scheme.

611

612 **Scheme 2.** Transformation of compound 4 into compound 5 via sunlight radiation.

613

614 **Scheme 3** Coordination modes of the p-hydroxycinnamate ligand found in the presented structures.  
615 Note that the phenol group in coordination mode (d) is deprotonated.

616

617 **Figure. 1.** (A) Monomers 1A (left) and 1B (right), and their corresponding numbering scheme for  
618 relevant atoms. Only hydrogen atoms participating in H-bonds are shown. (b) View of the H-bond  
619 interaction in each individual chain (A left, B right). View along the c axis. (c) 3D stacking of  
620 monomers 1A and 1B. View along the b axis.

621

622 **Figure. 2.** (A) Polymers 2 (top) and 3 (down): their corresponding numbering scheme for relevant  
623 atoms. Only phenolic hydrogens are shown. (B) Polymeric 2D layers of compounds 2 (left) and 3  
624 (right).

625

626 **Figure. 3** A) Perpendicular cut of the 2D layers for 2 (left) and 3 (right). (B) H-bond interactions  
627 forming the supramolecular structure of 2 (top-left). Details of the main H-bonding holding the layer  
628 together (top-right). H-bond interactions forming the supramolecular structure of 3 (bottom-left). Details  
629 of the main H-bonding holding the layer together (bottom-right).

630

631 **Figure. 4** A) Schematic representation of the channels occupied by the solvent molecules in 3. (b)  
632 PXRD pattern from 3 simulated from the resolved structure (single crystal XRD measured at 100 K,  
633 bottom). PXRD diffractogram of 3 measured at room temperature after exposure to air (middle-bottom).  
634 PXRD diffractogram of 3 measured at room temperature after exposure to a saturated MeOH  
635 atmosphere (middle-top). PXRD of the remaining powder after vacuum exposure of 3 (top).

636

637 **Figure. 5** A) Dimer 4A (top) and monomer 4B (down), and their corresponding numbering scheme for  
638 relevant atoms. Only phenolic hydrogens are shown. (B) Perpendicular view of the 2D layer formed by  
639 dimer 4A (yellow) and monomer 4B (green).

640

641 **Figure. 6** H-bond interactions forming the supramolecular structure of 4. Dimer centred view (top) and  
642 monomer centred view (bottom)..

643 **Figure. 7** Schematic representation of the cavities occupied by solvent  
644 molecules in 4.

645  
646 **Figure. 8** (A) Polymeric 1D chain of compound 5. (B) Corresponding dimeric subunits 5-trans (top) and  
647 5-cis (down) with their corresponding numbering scheme. Only phenolic hydrogens are shown.

648  
649 **Figure. 9** A) View of the 3D supramolecular structure in 5. (B) Details of the supramolecular  
650 interactions in 5.

651  
652 **Figure. 10** Thermal variation of  $\chi_{pT}$  for 5. The solid red line is the best fit to the proposed model (see  
653 text)..

654

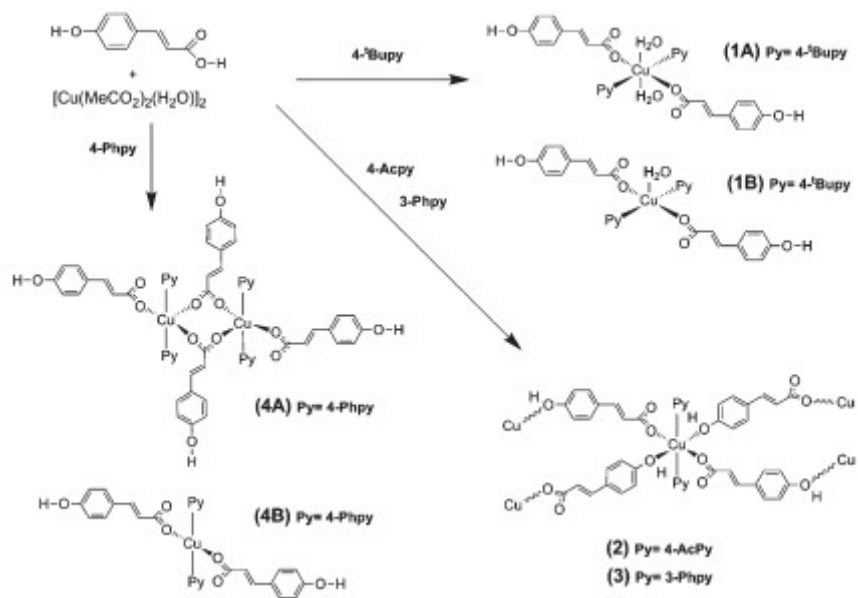
655

656



657  
658  
659  
660

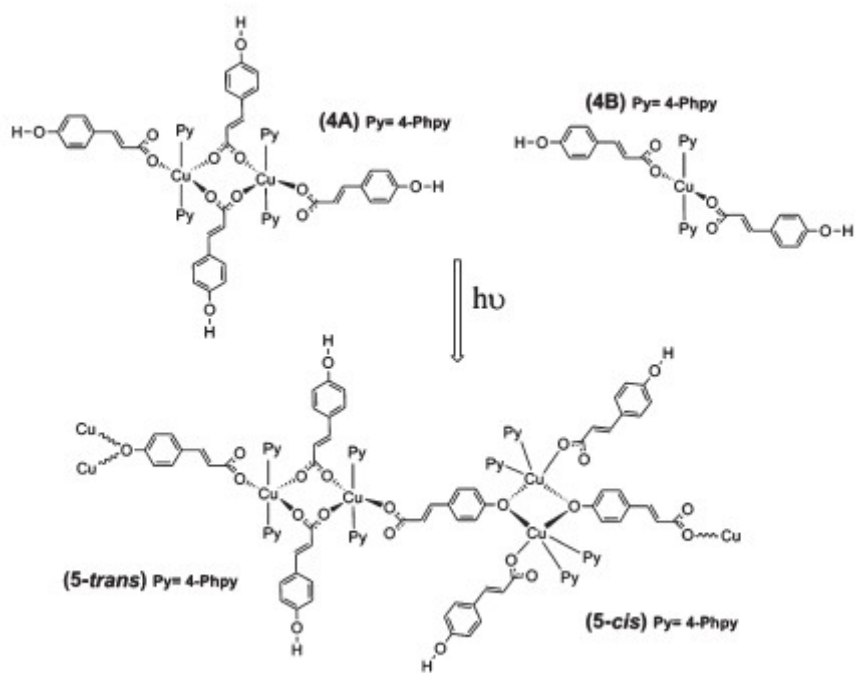
### SCHEME 1.



661  
662

663  
664  
665

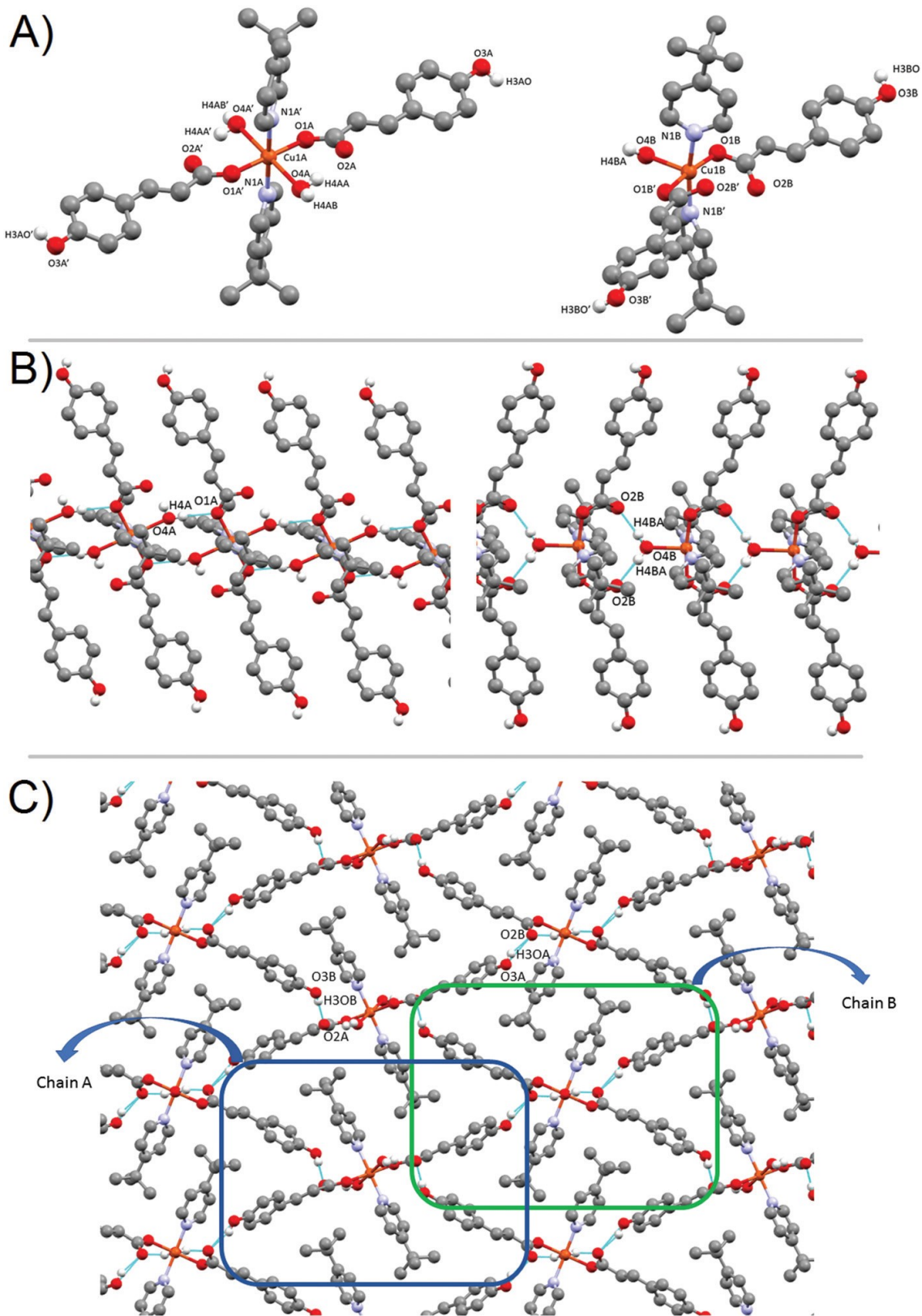
SCHEME 2.



666  
667  
668

669  
670

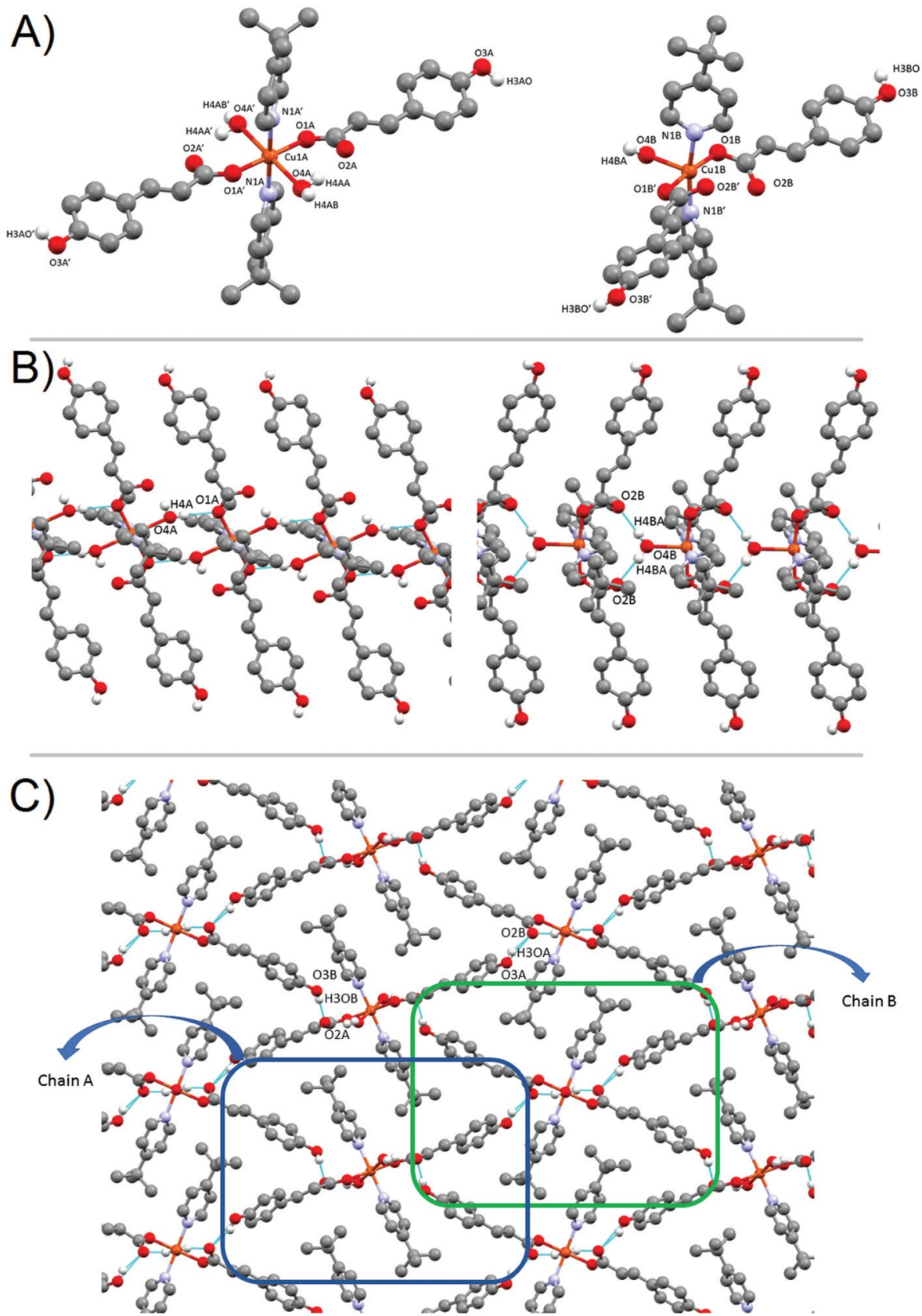
FIGURE 1



671  
672  
673

674  
675

FIGURE 2

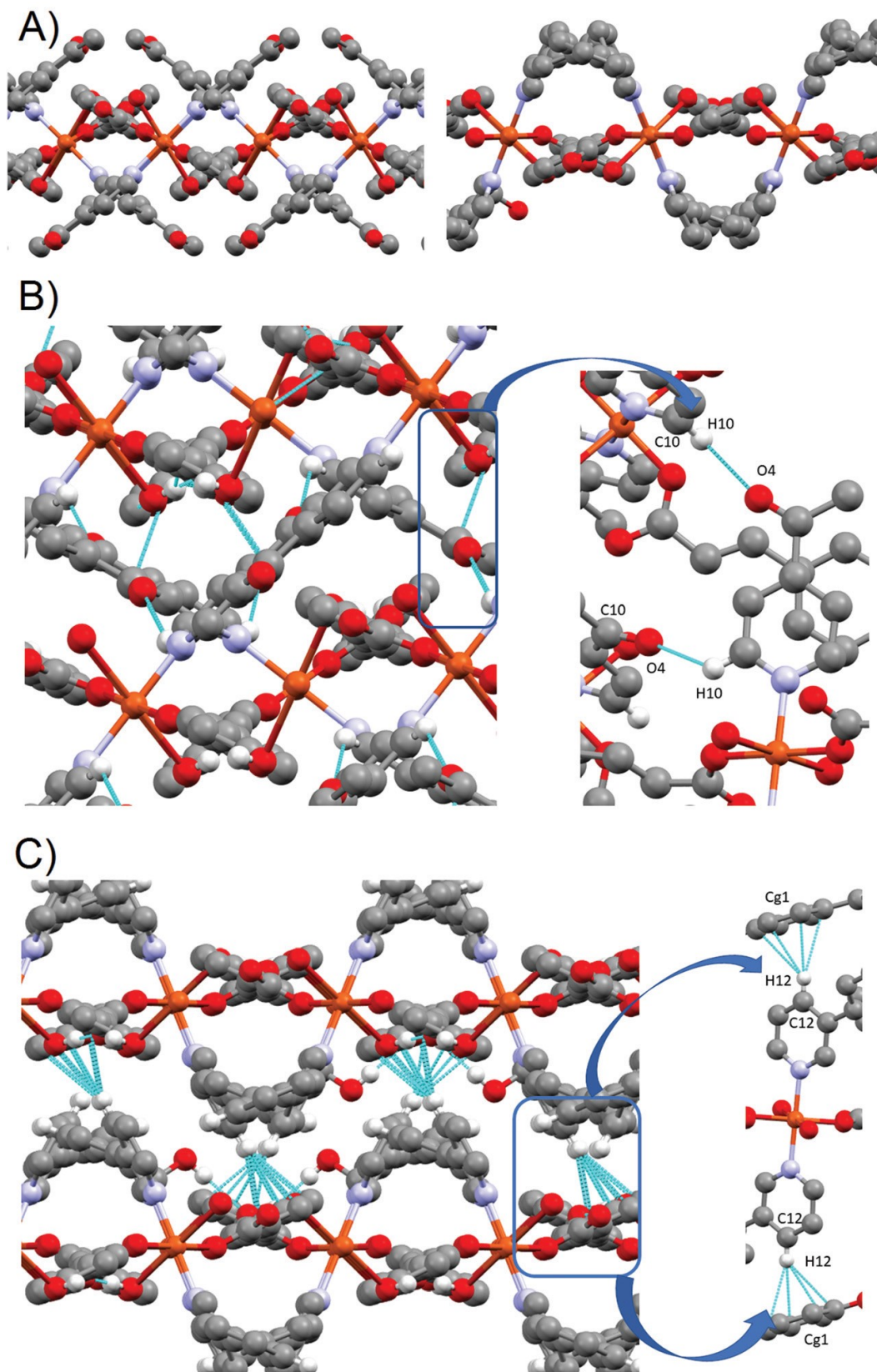


676  
677  
678



679  
680

FIGURE 3



681  
682



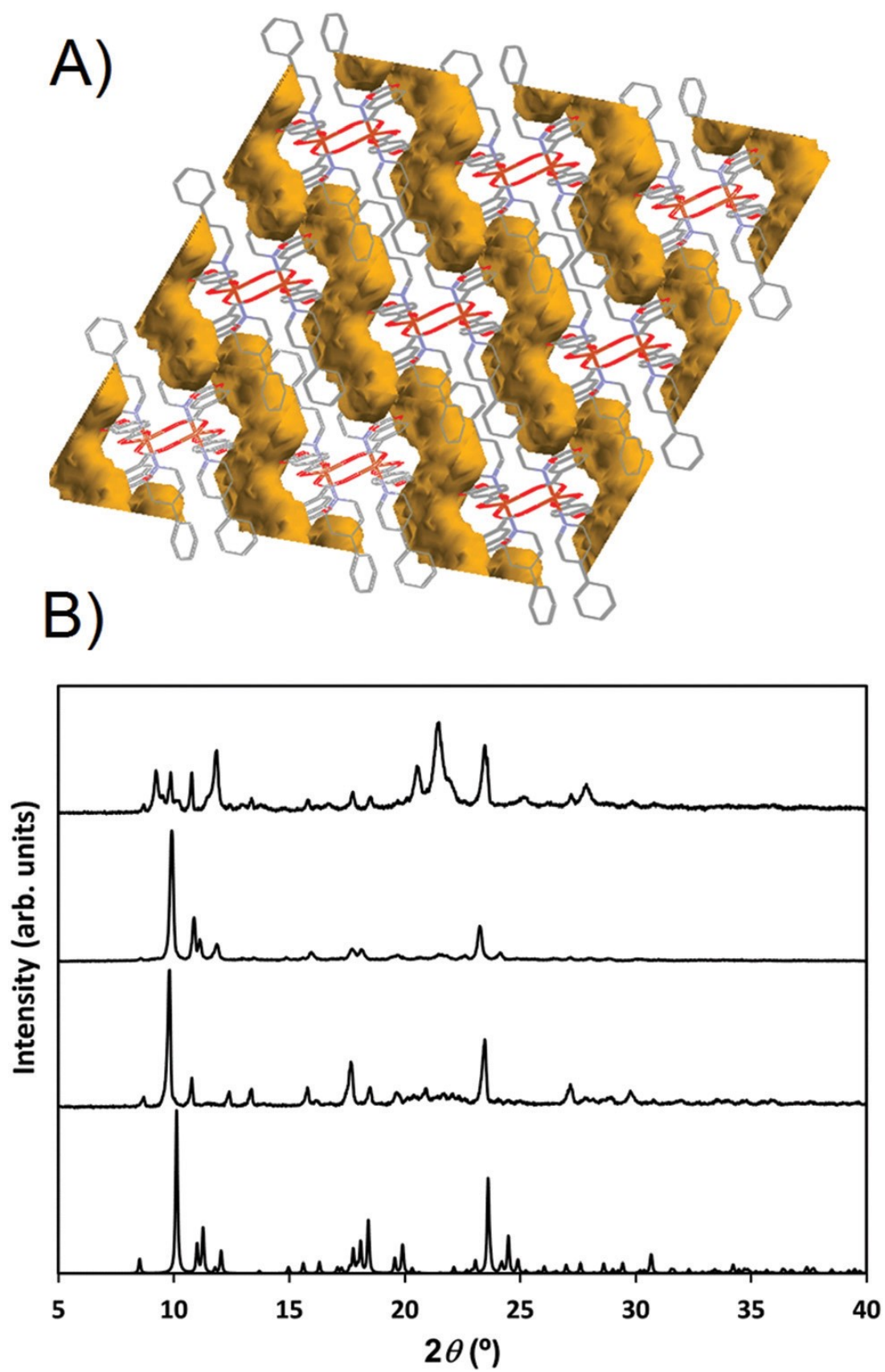
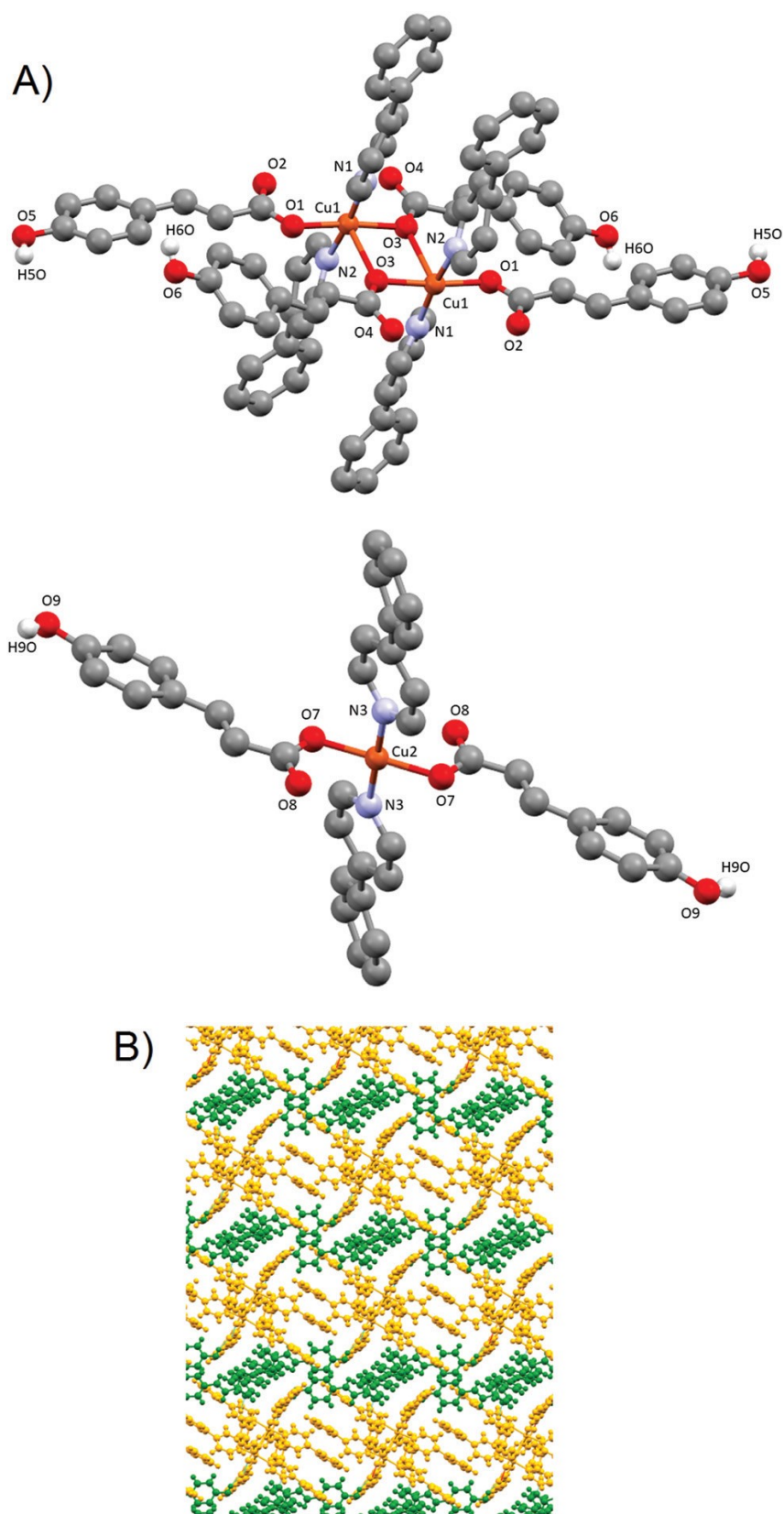


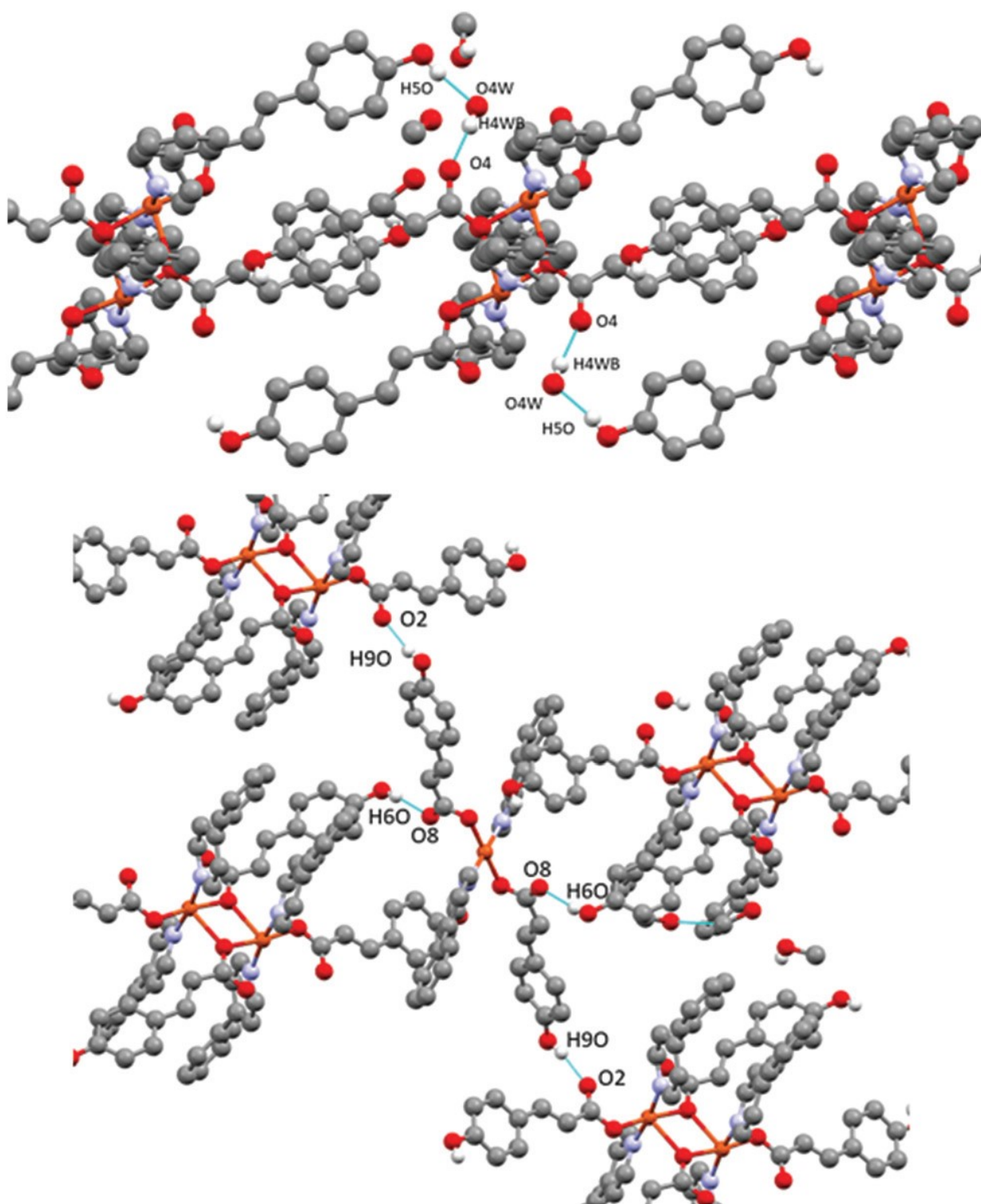
FIGURE 5.





691

FIGURE 6.



692

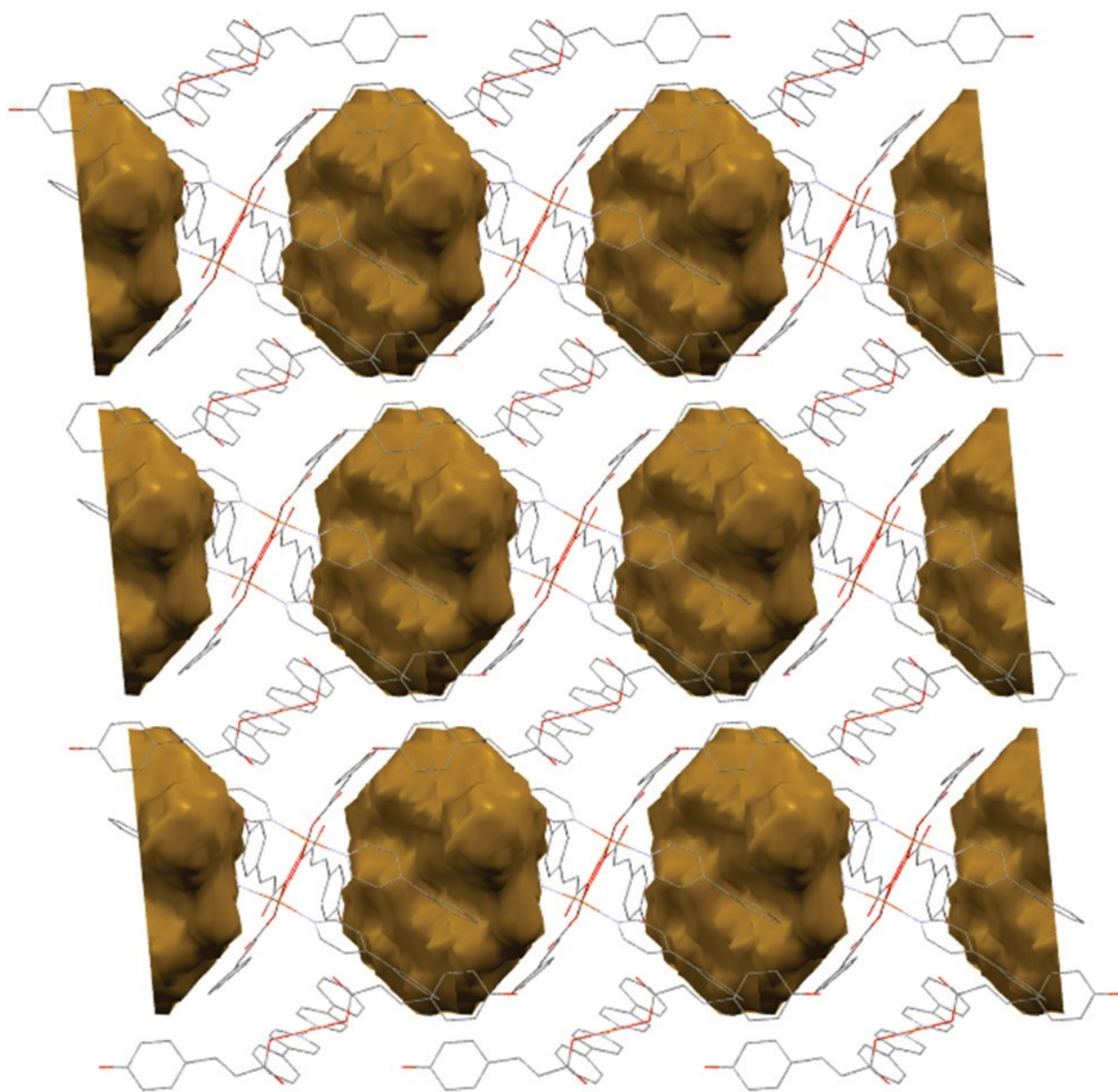
693

694

695

FIGURE 7.

696



697

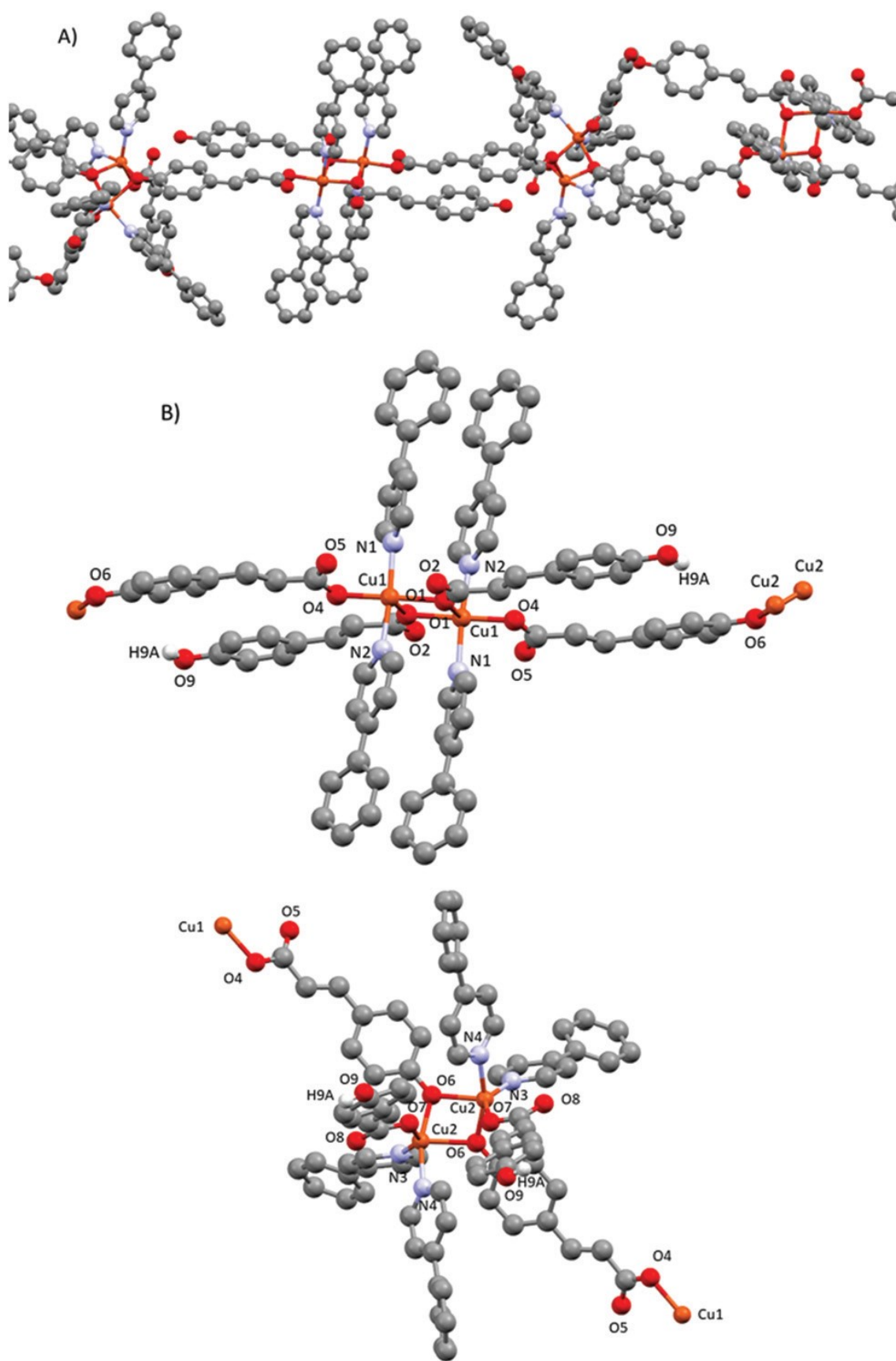
698

699

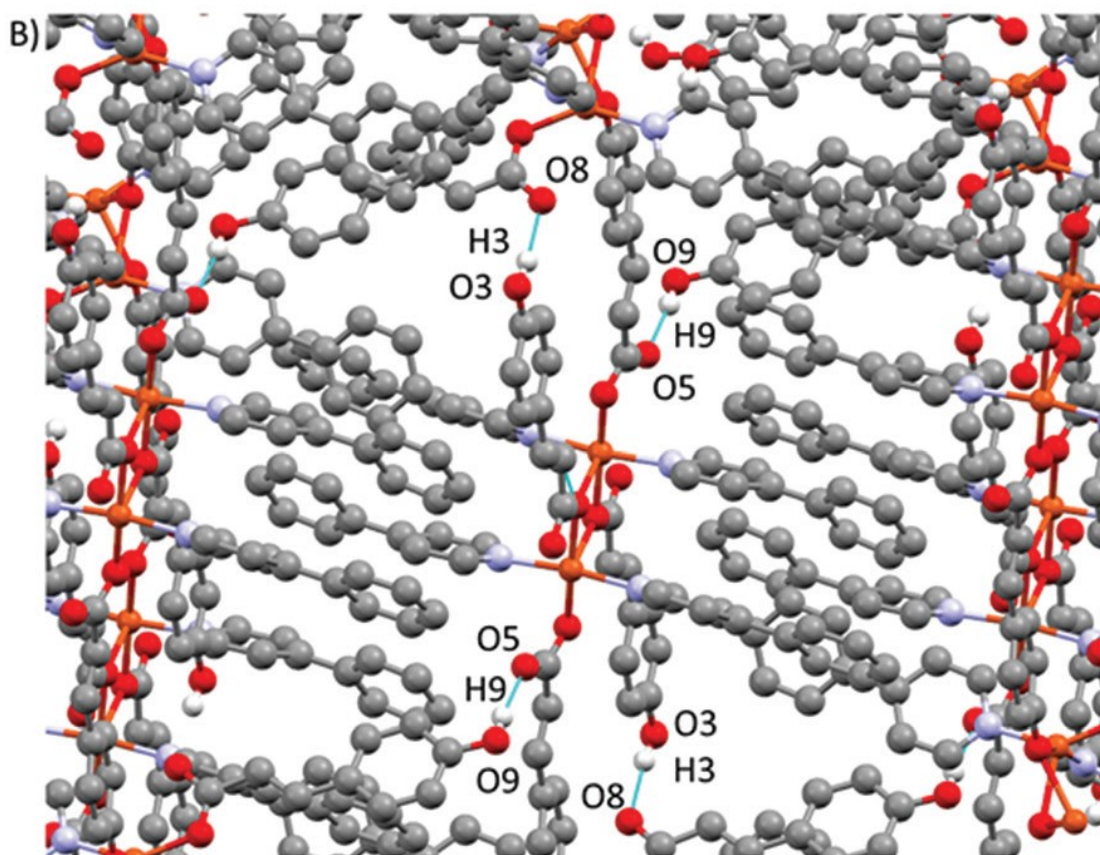
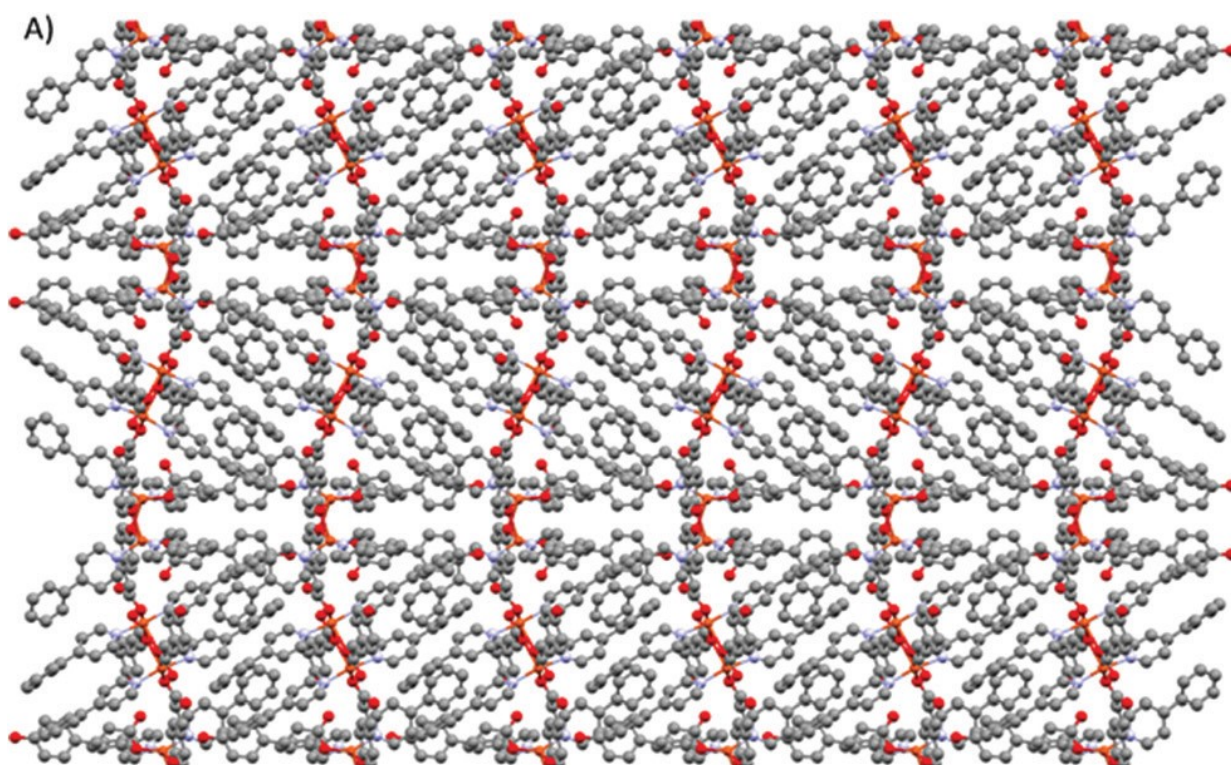
700

701

702





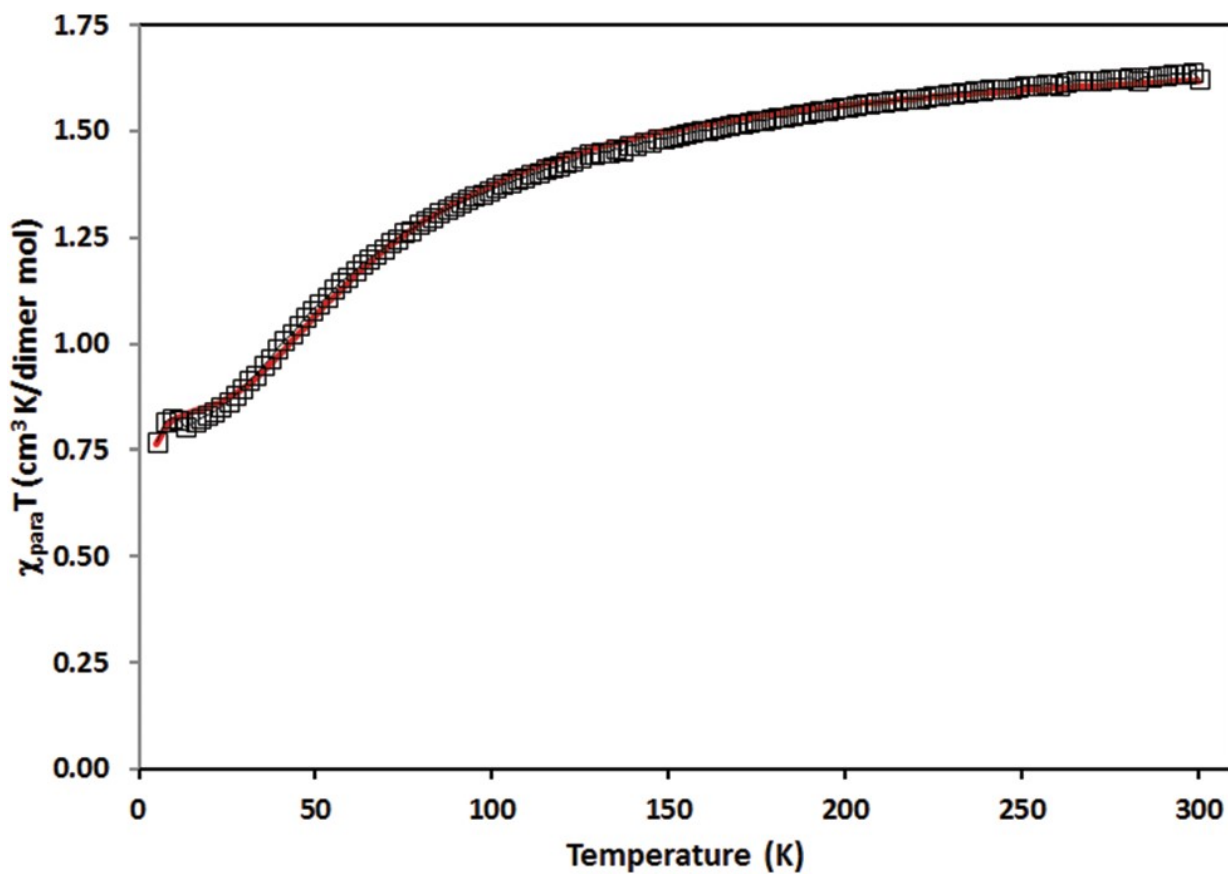


709

FIGURE 10.

710

711



712